Department of Mechanical Engineering
The Pennsylvania State University
University Park, Pennsylvania

Flame Trajectory and Its Experimental Determination in Vortex Combustion

Technical Report No. 2
Vortex Controlled Multifuel Combustion
Contract No. DA-36-034-ORD-3366T
U. S. Army Materiel Command
Army Tank-Automotive Center

May 1963

Prepared by:

Yongson Lee
Graduate Assistant in
Mechanical Engineering

Approved by:

W. E. Meyer
Professor of
Mechanical Engineering

Abstract

A rotating, cylindrical combustion chamber was used to observe the effect of chamber rotative speed and location of the point of ignition on combustion duration and flame trajectory in a cylindrical force field. Experimental trajectories of the flame in homogeneous and nonhomogeneous mixtures were compared with analytically obtained ones. The study lead to the following conclusions:

1. The optimum location of the point of ignition is at the periphery of the combustion chamber for both, homogeneous and nonhomogeneous, gas mixtures because this flame origin produces the strongest vortex.

2. Combustion of a nonhomogeneous gas mixture provides greater time rates of energy emission than that of a homogeneous mixture. Combustion of a homogeneous mixture, however, produces a stronger swirl than that of a nonhomogeneous mixture when both are overrich.

3. At the beginning of the combustion the experimentally observed trajectories of the flame coincide with the theoretically determined trajectories, but in the later portion of the combustion they do not because the drag on the inflamed portion of the mixture exceeds that predicted by theory.

ACKNOWLEDGMENT

The author wishes to express his sincere appreciation to Professors W. E. Meyer and A. W. Hussmann for their continuous advice and counseling throughout the course of the project. The author is also greatly indebted to Dr. H. Kakimoto whose advice and suggestions until his untimely death were most valuable. The author wishes to thank Daniel A. Willis, Research Assistant, for his kind help, particularly in matters of style, syntax, and grammar.

Thanks are also due W. M. Glass, P. E. Stephens, and other members of the Technical Services staff who contributed immeasurably to the success of this thesis by constructing, or making available, the necessary apparatus and equipment.

TABLE OF CONTENTS

TABLE OF CONTENTS, Continued

LIST OF TABLES

LIST OF FIGURES

LIST OF FIGURES, Continued

LIST OF FIGURES, Continued

NOMENCLATURE

Symbol	Quantity	Units
A	Projected area of the flame	$in.^2$
a_0	Acceleration for fixed coordinate of the particle	$in./sec^2$
C_D	Drag coefficient	———
D	Diameter of the flame	in.
F_a	Inertia force	lb_f
F_D	Drag force	lb_f
F_P	Pressure force	lb_f
h	Height of the combustion chamber	in.
i	Unit vector of x axis	———
j	Unit vector of y axis	———
k	Unit vector of z axis	———
m_f	Mass of the flame	lb_m
P_0	Initial pressure in combustion	$lb_f/in.^2$
P	Pressure at arbitrary time in combustion	$lb_f/in.^2$
P_e	Final pressure in combustion	$lb_f/in.^2$
r_0	Radial distance between geometrical center and center of the flame	in.
r	Radial distance	in.
R	Radius of the flame	in.
R_c	Radius of the combustion chamber	in.
Re	Reynolds number	———
V	Volume of the flame	$in.^3$
V_0	Tangential velocity of particle in fixed coordinates	in./sec

NOMENCLATURE, Continued

Symbol	Quantity	Units
V_{rel}	Relative velocity of the flame	in/sec
x	Real value of fixed coordinates	in.
y	Value of imaginary part of fixed coordinates	in.
x_0	Real position of the spark plug for fixed coordinates	in.
y_0	Value of imaginary position of the spark plug for fixed coordinates	in.
$\bar{z}$	Position vector of the flame center for fixed coordinates	———
γ	Specific heat ratio of mixture	———
ρ_a	Density of air-acetylene mixture	$lb_f/in.^3$
ρ_f	Density of the flame	$lb_f/in.^3$
μ	Viscosity of the mixture	lb_m / in.sec
$\bar{\eta}$	Position vector of flame center for rotational coordinates	———
ξ	Real value for rotational coordinates	in.
η	Value of imaginary part of rotational coordinates	in.
ξ_o	Real value of the spark plug for rotational coordinates	in.
η_o	Value of imaginary part of the spark plug for rotational coordinates	in.
ω	Angular velocity of the chamber	rad/sec

I. INTRODUCTION

1.1 General Statement of the Problem

In recent years, several investigators have pointed out that in a vortex type combustion chamber the inflamed gas particles, being of lower density than the surroundings, have the tendency to move spirally toward the center of the chamber under the influence of the centrifugal force field of the air swirl. If we are to enter into the field of research pertaining to the thermal mixing effect of gases, then it is necessary to know the flow pattern, at least up to the moment at which combustion starts, since all further particle motion will be governed by the existing flow patterns. It is difficult to predict the flow pattern in an actual engine because the moving piston produces transient flows that result in random turbulence. Also, there are wall effects that at present are not fully understood.

It is possible to eliminate the effect of the combustion chamber wall by rotating the chamber at constant speed and thus produce a flow pattern which approaches that of perfect solid body rotation. For this reason, this study was undertaken using a rotating cylindrical combustion chamber in order to determine the trajectory of the flame. It was considered of value to study the effect of chamber speed and spark plug position on the combustion time in both homogeneous and nonhomogeneous gas mixtures. In order to observe and study these phenomena, flame photographs were taken with a high speed camera.

The ultimate object of the study was to compare the theoretical and experimental flame trajectories, that is, the locus of the center of the flame. The assumption was made that only the pressure force due to the centrifugal action and the drag force on the flame significantly influence its path. Magnetic forces and other miscellaneous effects were neglected since the chamber was not operated at elevated temperatures.

1.2 Previous Related Studies

F. and A. Pischinger (1)* treated this phenomenon theoretically on the assumption that the air rotation consists of a free vortex. They came to the conclusion that the trace of the flame is a logarithmic spiral, the angle of which depends on the ratio of burnt gas density to that of the unburnt gas, and also that the angle is independent of the swirl speed. F. Nagai and H. Kakimoto (2) investigated a spiral curl of flame in a swirl chamber and discussed the reason why better combustion results when the fuel was injected in the direction of the air swirl rather than against it. J. S. Meurer (3) emphasized in a recent paper that the thermal mixing effect was one of the most important factors that let the M-system approach the ideal combustion process. Eisfeld (4) determined the trajectory of droplets within the Stoke's regime in a swirling field. The problem of describing the trajectories of particles has also been solved by Kriebel (5) by means

*Numbers in parentheses designate References in Bibliography.

of the Laplace transformation under the assumptions that there is a density difference between the surroundings and the particles and that the only factors that affect the trajectories are the pressure forces due to the centrifugal action and the drag forces. Calder (6) investigated the motion of a heavy spherical particle in the rotating cylinder. He assumed that the viscous drag on the particle was given by the Stokes resistance formula, and that the fluid rotated as a solid body.

The flow pattern in a model chamber with a tangential inlet passage was observed and measured by A. W. Hussmann and F. Kahoun (7) who determined that the flow was one of solid body rotation and was not stable.

1.3 Origin of the Study

A few theoretical studies have been published relative to the combustion of a uniform mixture in a static vessel. S. D. Raezer (8) calculated the relationship between burning velocity and space velocity of a spherical wave in a fixed and closed spherical chamber. A. S. Campell (9) studied the required combustion time for constant volume combustion in the one-dimensional case. F. Nagao et al (10) discussed the flame development in a swirl with solid body rotation. D. G. Udelson (11) experimentally studied the effect of a single sphere of burning vapors resulting from a drop of liquid fuel in an undisturbed air stream, but he did not consider the force effects due to an unbalanced system, nor did he investigate flame development in a wheel-type swirling field.

Thermal mixing is an important factor in the improvement of fuel stratification and combustion. The effect of thermal mixing on combustion is known to be related to the swirling motion of the field (12). After ignition, this swirl will be intensified by the flame motion. Therefore, one important factor in investigating the thermal mixing is to find the trajectory of the flame in a swirling field after ignition has occurred.

In this investigation the effect of radial unbalance was included in the theoretical determination of the flame trajectory for both fixed and rotational coordinates under the assumptions of solid body rotation and negligible wall effect. The flame trajectory was also investigated by experimental methods.

II. THEORETICAL CONSIDERATIONS

2.1 Statement of the Problem

In this investigation an analysis has been made of the flame trajectory in a rotating combustion chamber model during the combustion process. The problem is very difficult to analyze precisely because of the many unknown functions of time. For example, the relationships between pressure and time and between the radius of the flame and time are important factors in finding the flame trajectory, but these relationships are very difficult to obtain analytically and must be determined experimentally. Von Elbe (13), using the concept of burning fraction which was derived by A. S. Campell (9) has analytically predicted the radius of a spherical flame under the assumption that the flame expands adiabatically. Von Elbe's (13) equation cannot be used for the present problem because the relationship between pressure and time is an unknown function. In this study the wall effect was neglected, that is, the derivation that will be presented holds only until the flame front reaches the cylinder wall.

Since the drag coefficient is an unknown function of the Reynolds number, the relationship between drag coefficient and Reynolds number was approximated in the present analysis by a piecewise logarithmic-linear relation. In the latter portion of the combustion time, as shown in Fig. 2.1, indistinct boundaries between the flame and its surroundings occur. The flame core consists of decomposition products of acetylene and air, and the amorphous portion may be considered to be a kind

of flame diffused from the flame core. After the flame grows to an order of magnitude comparable to that of the combustion chamber, drag force is no longer proportional to the square of relative velocity. Therefore, we cannot apply the piecewise logarithmic linear relationship to this situation; thus the assumed relationship between drag coefficient and Reynolds number does not hold for the later portion of the combustion period.

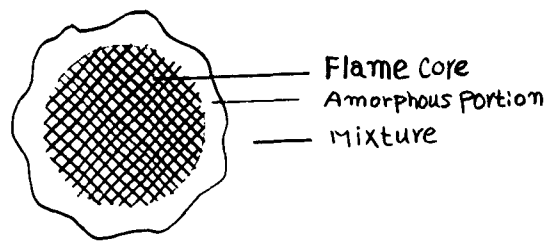

Fig. 2.1. Schematic diagram of the growing flame

2.2 Assumptions

In the following simplified analysis, the resulting flame trajectory of an acetylene-air mixture injected into a rotating cylindrical chamber filled with air and ignited by a spark plug has been investigated under the following assumptions:

1. The flame is two-dimensional; in other words, combustion flame spreads only in the plane perpendicular to the axis of the combustion chamber.
2. The radius of the flame is constant over a small interval of time.

3. The angular velocity of the chamber is constant.
4. The boundary line between the flame and its surrounding is distinct.
5. The flame moves through an acetylene-air mixture that is homogeneous and rotates as a solid body.
6. Magnetic forces are negligible.

2.3 Derivation

The equation of equilibrium is as follows:

Inertia force = drag force + radial pressure force

$$F_a = F_D + F_p$$

Pressure force: When the flame size is small, the pressure gradient in the radial direction is $\rho_a r\omega^2/g$. When the flame grows to a size comparable to the chamber size, the pressure force in a radial direction must be obtained by a different analysis.

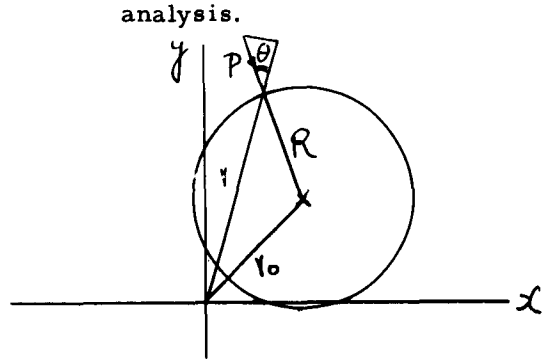

Fig. 2.2. Radial pressure force diagram for large flame size.

As noted in Fig. 2. 2, since the circumferential and axial pressure gradients are negligible, one can obtain the radial pressure force applied to the flame from the Navier-Stokes equation in cylindrical coordinates.

The radial pressure gradient is $\frac{dP}{dr} = \frac{\rho_a r \omega^2}{g}$

or

$$P = \frac{1}{2g} \rho_a r^2 \omega^2 + C$$

Letting P be the pressure above the pressure at the geometrical center, then

$$C = 0$$

Now the pressure force is given by

$$F_P = \oint P \cos\theta \, dA$$

where

$$dA = R h \, d\theta$$

Therefore

$$F_P = 2 \int_0^{\pi} \frac{1}{2g} \rho_a r^2 \omega^2 R h \cos\theta \, d\theta$$

$$= \frac{\pi \rho_a R^2 h r_0 \omega^2}{g}$$

The flame volume is given by

$$V = \pi R^2 h$$

Therefore the radial pressure force can be expressed as

$$F_P = \frac{1}{g} \rho_a V r_0 \omega^2$$

Thus, even in the case of a large size flame, the same equation for the radial pressure force can be used as in the case of a small size flame.

The drag force is given by

$$F_D = \frac{1}{2g} \rho_a A C_D V_{rel}^2$$

Since the drag force and the pressure force are directed inward toward the geometrical center, the equation of equilibrium can be rewritten as

$$F_a = -F_D - F_p$$

The mass of the flame is

$$m_f = \frac{1}{g} \rho_f \pi R^2 h$$

Therefore, the equilibrium equation can be shown to be

$$m_f \frac{d^2\bar{z}}{dt^2} = -\frac{\rho_a R h C_D}{g} \overline{V_{rel}}^2 - \frac{\rho_a \pi R^2 h}{g} \bar{z} \omega^2$$

Dividing both sides of m_f results in the following expression for the acceleration of the flame:

$$\frac{d^2\bar{z}}{dt^2} = -\frac{C_D \rho_a}{\pi R \rho_f} \overline{V_{rel}}^2 - \frac{\rho_a}{\rho_f} \bar{z} \omega^2 \qquad \text{Eq. 2.1}$$

Now

$\frac{\rho_a}{\rho_f} \cong 3.0$ for the acetylene-air mixture flame; therefore, in this case, Equation 2.1 is as follows:

$$\frac{d^2\bar{z}}{dt^2} = -\frac{3C_D}{\pi R}\bar{V}_{rel}^2 - 3\bar{z}\omega^2 \qquad \text{Eq. 2.2}$$

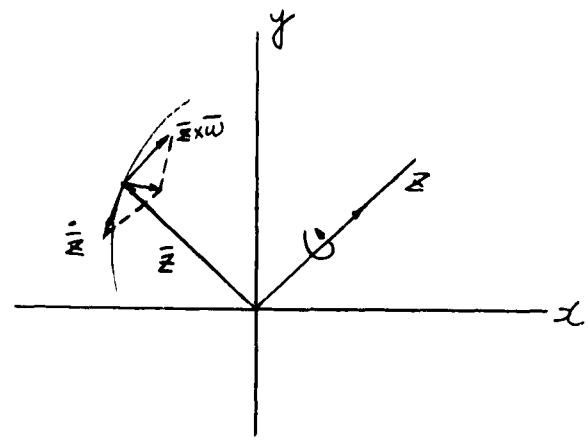

Fig. 2.3 Vector diagram for relative velocity of the flame.

As obtained from Fig. 2.3, the relative velocity of the flame can be expressed as

$$V_{rel} = \dot{\bar{z}} + \bar{z}\times\bar{\omega} \qquad \text{Eq. 2.3}$$

But

$$\bar{z}\times\bar{\omega} = (ix+jy)\times\omega k$$
$$= -i\omega x + \omega y \qquad (i=\sqrt{-1})$$
$$= -i\bar{z}\omega \qquad \text{Eq. 2.4}$$

Substitution of Equation 2.4 into Equation 2.3 results in:

$$V_{rel} = \dot{\bar{z}} - i\bar{z}\omega$$

Substitution of this relation into Equation 2.2 results in the following expression for the acceleration of the flame

$$\frac{d^2\bar{z}}{dt^2} = -\frac{3C_D}{\pi R}\left|\dot{\bar{z}} - i\bar{z}\omega\right|\left(\dot{\bar{z}} - i\bar{z}\omega\right) - 3\bar{z}\omega^2 \qquad \text{Eq. 2.5}$$

If one changes to a rotational coordinate system, the tangential velocity, which is given by $\frac{d\bar{z}}{dt} = V_0$ in the fixed coordinate system, will be modified as follows

$$\frac{d\bar{z}}{dt} = \left(\frac{dx}{dt}i + \frac{dy}{dt}j + \frac{dz}{dt}K\right) + \left(\frac{di}{dt}x + \frac{dj}{dt}y + \frac{dK}{dt}z\right)$$

$$= \dot{\bar{\eta}} + \omega \times \bar{\eta}$$

$$= \dot{\bar{\eta}} - \bar{\eta} \times \bar{\omega}$$

Then for the two dimensional case

$$\frac{d\bar{z}}{dt} = \dot{\bar{\eta}} + i\omega\bar{\eta}$$

The acceleration for the fixed coordinate system is given by:

$$a_0 = \frac{d^2\bar{z}}{dt^2}$$

$$= \ddot{\bar{\eta}} + 2\omega \times \dot{\bar{\eta}} + \bar{\omega} \times (\bar{\omega} \times \bar{\eta}) + \dot{\bar{\omega}} \times \bar{\eta}$$

In the present problem

$$\dot{\bar{\omega}} = 0$$

Therefore, for the two dimensional case

$$a_0 = \ddot{\bar{\eta}} + 2i\omega\dot{\bar{\eta}} - \bar{\eta}\omega^2$$

If one breaks the complex numbers into their real and imaginary parts, the results are:

$\bar{z} = x + iy$ for fixed coordinates

$\bar{\eta} = \xi + i\zeta$ for rotational coordinates

or

$$\bar{z} = \bar{\eta} e^{i\omega t}$$

therefore

$$\dot{\bar{z}} = (\dot{\bar{\eta}} + i\omega\bar{\eta}) e^{i\omega t}$$

Eq. 2.6

$$\ddot{\bar{z}} = (\ddot{\bar{\eta}} + 2i\omega\dot{\bar{\eta}} - \eta\omega^2) e^{i\omega t}$$

Eq. 2.7

Substitution of Equations 2.6 and 2.7 into Equation 2.5 will give:

$$(\ddot{\bar{\eta}} + 2i\omega\dot{\bar{\eta}} - \bar{\eta}\omega^2) e^{i\omega t} = -\frac{3C_D}{\pi R}|\bar{\eta}||e^{i\omega t}|\bar{\eta} e^{i\omega t} - 3\bar{\eta}\omega^2 e^{i\omega t}$$

Finally, there results in the rotational coordinate system

$$\ddot{\bar{\eta}} + 2i\omega\dot{\bar{\eta}} - \bar{\eta}\omega^2 = -\frac{3C_D}{\pi R}|\dot{\bar{\eta}}|\dot{\bar{\eta}} - 3\bar{\eta}\omega^2 \qquad \text{Eq. 2.8}$$

In Equation 2.8 the first term of the left side is an apparent acceleration term of the flame center. The second term of the left side is the Coriolis force component due to rotation.

The boundary conditions for Equation 2.8 are

$$\dot{\bar{\eta}} = 0 \quad at \quad t = 0$$

Since the axis through the point of ignition was taken as the real axis, the point of ignition is a real value. Therefore, for a cylinder of 2.5 inches diameter with the point of ignition midway between the periphery and the center

$$Re\,\bar{\eta} = 0.625, \quad Im\,\bar{\eta} = 0$$

Separating $\bar{\eta}$ into its real and imaginary parts, one has for the boundary conditions in the rotational coordinate system:

$$\dot{\xi}_0 = 0, \quad \dot{s}_0 = 0 \quad at \quad t = 0$$

$$\xi_0 = 0.625, \; s_0 = 0 \quad at \quad t = 0 \qquad (B)$$

Recalling Equation 2.5 and 2.6 in order to determine the boundary conditions in the fixed coordinate system

$$\bar{x} = \bar{\eta}\, e^{i\omega t}$$

$$\dot{\bar{x}} = (\dot{\bar{\eta}} + i\omega\bar{\eta})\, e^{i\omega t}$$

When $t=0$ one, therefore, has:

$$\bar{z}_0 = \bar{\eta}_0$$
$$\dot{\bar{z}}_0 = i\omega\bar{\eta}_0$$

Separating $\bar{z}_0$ and $\bar{\eta}_0$ into their real and imaginary parts, one has:

$$x_0 + iy_0 = \xi_0 + i\zeta_0$$
$$\dot{x}_0 + i\dot{y}_0 = i\omega(\xi_0 + i\zeta_0)$$

Therefore, the boundary conditions for fixed coordinates are:

$$\left.\begin{aligned} x_0 &= 0.625, \quad y_0 = 0 \quad \text{at } t = 0 \\ \dot{x}_0 &= 0, \quad \dot{y}_0 = 0.625\omega \text{ at } t = 0 \end{aligned}\right\} \quad (c)$$

To go further with Equations 2.5 and 2.8 we need to know the drag coefficient C_D; and since it is related to the Reynolds number, Re, it is necessary to find the Reynolds number which is given by the following expression.

$$Re = \frac{\rho a D}{\mu} |V_{rel}| \quad \text{because Re is a scalar value.}$$

But

$$V_{rel} = \dot{\bar{z}} - i\bar{z}\omega$$
$$= (\dot{x} + i\dot{y}) - i(x + iy)\omega$$

$$|V_{rel}| = [\bar{V}_{rel}\, \underline{V}_{rel}]^{\frac{1}{2}}$$

Where $\underline{V}_{rel}$ is the complex conjugate of $\bar{V}_{rel}$

Therefore, one has

$$|V_{rel}| = \{(\dot{x}+y\omega)^2+(\dot{y}-x\omega)^2\}^{\frac{1}{2}}$$

Using this expression for the relative velocity, Re is given by:

$$Re = \frac{\rho_a D}{\mu}\{(\dot{x}+y\omega)^2+(\dot{y}-x\omega)^2\}^{\frac{1}{2}} \text{ in fixed coordinates.}$$

Now in rotational coordinates:

$$V_{rel} = \dot{\eta}$$
$$= \dot{\xi} + i\dot{\zeta}$$

Therefore, the Reynolds number in rotational coordinates is given by:

$$Re = \frac{\rho_a D}{\mu}|V_{rel}|$$
$$= \frac{\rho_a D}{\mu}(\dot{\xi}^2+\dot{\zeta}^2)^{\frac{1}{2}}$$

It should be noted that μ, ρ_a and D are scalar values; thus these parameters are invariants in the coordinate transformation. Since the relationship between drag coefficient C_D and the Reynolds number Re for a cylindrical object is not defined by a simple function, this relationship was approximated

by a series of logarithmic linear functions as shown in Table 4.1 and Fig. 4.16.

If Equation 2.5 is separated into its real and imaginary parts, one has:

$$\left.\begin{aligned}\ddot{x} &= -\frac{3C_D}{\pi R}\sqrt{(\dot{x}+y\omega)^2+(\dot{y}-x\omega)^2}\,(\dot{x}+y\omega) - 3x\omega^2 \\ \ddot{y} &= -\frac{3C_D}{\pi R}\sqrt{(\dot{x}+y\omega)^2+(\dot{y}-x\omega)^2}\,(\dot{y}-x\omega) - 3y\omega^2\end{aligned}\right\} \text{Eq. 2.9}$$

Similarly, for Equation 2.8:

$$\left.\begin{aligned}\ddot{\bar{\eta}} &= -2i\omega\dot{\bar{\eta}} - \frac{3C_D}{\pi R}|\dot{\bar{\eta}}|\dot{\bar{\eta}} - 2\bar{\eta}\omega^2 \\ \ddot{\xi} &= 2\omega\dot{\zeta} - \frac{3C_D}{\pi R}\sqrt{\dot{\xi}^2+\dot{\zeta}^2}\,\dot{\xi} - 2\xi\omega^2 \\ \ddot{\zeta} &= -2\omega\dot{\xi} - \frac{3C_D}{\pi R}\sqrt{\dot{\xi}^2+\dot{\zeta}^2}\,\dot{\zeta} - 2\zeta\omega^2\end{aligned}\right\} \text{Eq. 2.10}$$

Equation 2.9 and 2.10 are the fundamental differential equations for this investigation; from these equations the tangential velocity, the position vector, and thus the trajectory of the flame can be calculated under the assumptions given in Section 2.2. It should be noted that in Equations 2.9 and 2.10, the flame radius R as a function of time must be calculated from measured values of the instantaneous combustion pressure P and from its final value P_e. Also C_D must be found from Re after finding $\frac{\rho_g D}{\mu}$ using measured values of P_e and P and combustion time.

Boundary conditions (B) for rotational coordinates apply to Equation 2.10.

Boundary conditions (C) for fixed coordinates apply to Equation 2.9.

To determine the radius of the flame for use in Equations 2.9 and 2.10, the method of B. Lewis and G. Von Elbe (13) used to derive an expression for the radius of a spherical flame was applied to a cylindrical flame. The derivation shown in Appendix I results in the following expression for the radius of the cylindrical flame:

$$R = R_c\left[1-(1-\eta)\left(\frac{P_o}{P}\right)^{\frac{1}{\gamma}}\right]^{\frac{1}{2}} \qquad \text{Eq. 2.11}$$

Where, as shown in Appendix I

$$\eta = \frac{P - P_o}{P_e - P_o} \qquad \text{Eq. 2.12}$$

P_o is the initial pressure of the mixture before ignition occurs.

Equation 2.12, derived from energy considerations and conditions in the burnt gas region, is valid only in the early stages of burning, in which the pressure rise is small. S. W. Raezer (8) has derived the final pressure P_e thermodynamically for combustion at constant volume, using average specific heats and dissociation equilibria. In the present study, P_e and P were measured by a pressure transducer and an oscilloscope. Thus

it is possible to calculate the flame radius R from E
using measured values of P.

Since the surrounding mixture will be compr
flame expands adiabatically, the temperature and d
mixture will also change adiabatically. Also, since
of the mixture is a function of the temperature, it w
from the air tables (neglecting the pressure effect).
ships between radius of the flame and time and betw
(recall the Reynolds number) and time were calcula
Equation 2.11 and the air tables. The change of ra
and of $\frac{\rho_a D}{\mu}$ will be described in detail in Cl

After the above factors were found, Equatio
were solved by numerical methods (Kutta-Simpson
with the aid of the University's digital computer, ar
The derivation of the numerical analysis for these e
shown in Appendix I; the computer program is show
II.

2.4 Hypothetical Considerations

In order to understand more clearly the for
we will consider two simplified, hypothetical cases

These cases are:

(1) The only force acting on the system
pressure force.

(2) The only force acting on the system
drag force.

One considers these cases in order to determine the relative magnitude of the pressure force and drag force acting on the flame.

Case 1

Consider the case in which the only force acting on the system is the pressure force. In this case, the equation of motion for a fixed coordinate system is given by

$$\ddot{\bar{z}} = -3\bar{z}\omega^2$$

Its solution is

$$\bar{z} = C_1 \exp(\sqrt{3}i\omega t) + C_2 \exp(-\sqrt{3}i\omega t)$$

The following results can be obtained by applying the boundary conditions for the fixed coordinate system, given in (C), to $\bar{z}$ and its first derivative:

$$C_1 + C_2 = 0.625$$

$$C_1 - C_2 = \frac{0.625}{\sqrt{3}}$$

$$C_1 = \frac{0.625}{2\sqrt{3}}(\sqrt{3}+1)$$

$$C_2 = \frac{0.625}{2\sqrt{3}}(\sqrt{3}-1)$$

$$\bar{z} = \frac{0.625}{2\sqrt{3}}[2\sqrt{3}\cos\sqrt{3}\omega t + 2i\sin\sqrt{3}\omega t]$$

$$x = 0.625\cos\sqrt{3}\omega t$$

$$y = \frac{0.625}{\sqrt{3}}\sin\sqrt{3}\omega t$$

If one rewrites the above equations, one has:

$$x^2 + 3y^2 = (0.625)^2$$

$$\text{or} \quad \frac{x^2}{(0.625)^2} + \frac{y^2}{(0.625/\sqrt{3})^2} = 1 \qquad \text{Eq. 2.13}$$

For a rotational coordinate system we have:

$$\xi = \frac{0.625}{\sqrt{3}}(\sqrt{3}.\cos\sqrt{3}\omega t.\cos\omega t + \sin\sqrt{3}\omega t.\sin\omega t)$$

Eq. 2.14

$$\zeta = \frac{0.625}{\sqrt{3}}(\sin\sqrt{3}\omega t.\cos\omega t - \sqrt{3}\cos\sqrt{3}\omega t.\sin\omega t)$$

If one writes Equation 2.13 in general form, the result is

$$\frac{x^2}{A^2} + \frac{y^2}{(A/\sqrt{B})^2} = 1 \qquad \text{Eq. 2.15}$$

where:

A = position of the spark plug

B = ρ_a/ρ_f

Case 2

Here the pressure force is neglected and only the drag force is assumed to be acting on the flame. In this case, the resulting equations of motion of the flame in rectangular coordinates are

$$\left.\begin{aligned}
\ddot{\bar{z}} &= -\frac{3C_D}{\pi R}\left|\dot{\bar{z}} - i\bar{z}\omega\right|\left(\dot{\bar{z}} - i\bar{z}\omega\right) \\
\ddot{x} &= -\frac{3C_D}{\pi R}\sqrt{(\dot{x}+y\omega)^2+(\dot{y}-x\omega)^2}\,(\dot{x}+y\omega) \\
\ddot{y} &= -\frac{3C_D}{\pi R}\sqrt{(\dot{x}+y\omega)^2+(\dot{y}-x\omega)^2}\,(\dot{y}-x\omega)
\end{aligned}\right\} \quad \text{Eq. 2.16}$$

Equations 2.16 were solved on the I.B.M. 7074 computer.

When the position of the spark plug is fixed and the density ratio of mixture to flame is increased, Equation 2.15 forms a family of elliptical curves. When $\frac{\rho_f}{\rho_a} \to \infty$, the flame motion is that of simple harmonic motion. A more detailed discussion is given in Chapter V.

III. EXPERIMENTAL APPARATUS AND PROCEDURE

The experimental studies were carried out in two phases. Phase I consisted of studies employing a homogeneous mixture combustion of methane and acetylene while in Phase II a non-homogeneous mixture combustion was used. The various tests conducted are summarized in Table 3.1. The tests in Phase I were conducted in five parts, of which (a) and (b) were explanatory tests. The tests in Phase II were conducted in three parts. These are described in more detail later; however, as noted, these tests were conducted to determine the effect of the combustion of various mixtures and conditions of combustion on combustion time and the trajectory of the flame.

The combustion time is defined in the present work as the interval between the time of ignition and the time the combustion pressure reached its maximum value. The combustion time was adopted as one of the important factors in the present study for the following reason. From the definition of heat of combustion, it can be shown that the higher the time rate of the combustion pressure is, the higher the time rate of energy emission from the combustion becomes. Therefore, for a constant maximum combustion pressure, the time rate of the combustion pressure becomes almost inversely proportional to the combustion time as defined above. During the initial stage of the experimental investigation, the maximum combustion pressure was found to be constant as long as the amount of flammable gas mixture charged into the combustion chamber was fixed. Consequently it was decided

TABLE 3.1. SUMMARY OF EXPERIMENTS

		Title	Class	Type of Fuel	Mixture: Charging Pressure of Fuel (in. of Hg.)	Mixture: Charging Pressure of Air (in. of Hg.)	Mixture: Fuel to Air Mixture Ratio	Mixture: Charging Amount of Mixture	Spark Plug Location	Charging Port
Phase I	Homogeneous mixture combustion Preliminary tests	Combustion pressure at different rotative chamber speeds	a	Methane	None	None	1:10 (volume)	Three times of the volume of chamber	Periphery	
		Photograph of flame development in the rotative combustion chamber	b	Acetylene	None	None	1:7 (volume)	Three times of the volume of chamber	Periphery	
		Effect of location of the point of ignition and rotative combustion chamber speed on combustion time	c	Methane	None	None	1:10 (volume)	Three times of the volume of chamber	Periphery, Half radius from center, Center	
		Experimental determination of flame trajectory	d	Acetylene	19	29.92	1:1.74 (weight)	0.316×10^{-4} lb	Half radius from center	
		Comparison of the effect of rotative chamber speed on combustion time for homogeneous and nonhomogeneous mixture combustion. Homogeneous mixture combustion.	e	Acetylene	10	43.92	1:4.85 (weight)	0.3×10^{-4} lb	Periphery	
Phase II	Nonhomogeneous mixture combustion	Effect of location of the point of ignition and rotative chamber speed on combustion time	f	Acetylene	10	43.92	1:4.85 (weight)	0.3×10^{-4} lb	Periphery, Half radius from the center, Center	Periphery Half radius from the center
		Comparison of the effect of rotative chamber speed on combustion time for homogeneous and nonhomogeneous mixture combustion. Nonhomogeneous mixture combustion	g	Acetylene	10	43.92	1:4.85 (weight)	0.3×10^{-4} lb	Periphery	Periphery
		Experimental determination of flame trajectory	h	Acetylene	3	29.92	1:11 (weight)	0.09×10^{-4} lb	Half radius from the center	Periphery

to use combustion time as a parameter indicating the time rate of energy emission which undoubtedly is one of the most important factors in the study of combustion.

3.1 Apparatus and Experimental Procedure for Phase I.

3.1.1 Mechanical Apparatus

In Phase I, an investigation was made of the effect of combustion chamber rotative speed and location of the point of ignition on combustion time and maximum pressure and of the flame trajectories. In order to determine accurately the flame trajectory by experimental methods, the equipment was designed so that all conditions in the combustion chamber would be as true as possible to the assumptions made for the analytical solution of the flame trajectory, namely, solid body rotation and negligible wall effect. Figure 3.1 is a schematic of the setup used for two parts of the investigation of the homogeneous mixture combustion. The first part concerns the effect of the combustion chamber rotative speed and location of the point of ignition on both combustion time and pressure, and the second part concerns the flame trajectory.

Combustion Chamber:

Since only a small amount of methane-air or acetylene-air mixture was injected into the combustion chamber at room temperature and atmospheric pressure, and since combustion was effected only intermittently, the strength of the combustion chamber was no serious problem. During the conduct of the test, the maximum

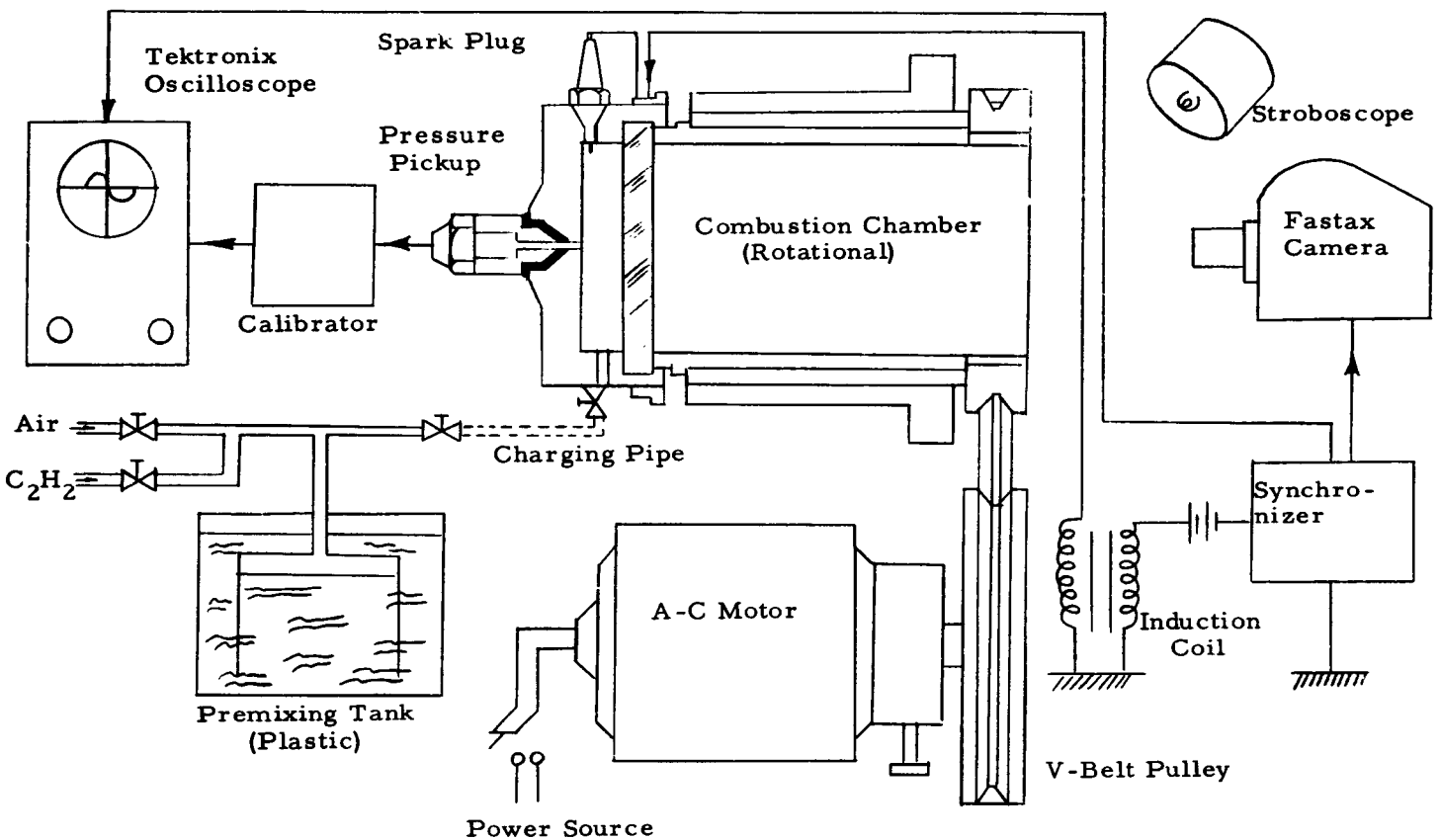

FIG. 3.1. EXPERIMENTAL SETUP FOR THE HOMOGENEOUS MIXTURE COMBUSTION.

chamber pressure encountered was approximately 140 pounds per square inch and the maximum chamber temperature approximately 230 degrees Fahrenheit.

Figure 3.2 shows a cross-section of the combustion chamber used for the homogeneous mixture combustion studies. The combustion chamber was made of ordinary steel, cylindrical in shape, 2.5 inches inside diameter and 0.5 inches long. One end of the combustion chamber was made of Lucite so that the flame could be photographed with a Fastax camera. Aniline, which was added to the fuel to increase the brightness of the flame, reacts chemically with Lucite; therefore, a piece of glass was placed over the Lucite on the inside of the chamber. In order to prevent leakage around the glass window, a rubber gasket was inserted between the combustion chamber and the glass window; and the joint around the glass and Lucite was sealed with putty. The other end of the chamber was steel and had a smooth counterbored hole for the insertion of a pressure pickup mounted in a fixed holder as shown in Fig. 3.2.

Figure 3.2 is a photograph of an exploded view of the combustion chamber. Spark plugs and valves were symmetrically inserted to provide for good balance as the chamber was rotated at speeds up to 3600 rpm. Only one of the spark plugs was used, however, while the others were inserted for balancing only. Since the combustion chamber was small, the combustion pressure was essentially uniform throughout the entire chamber; therefore, the indicated pressure at the center of the combustion chamber where

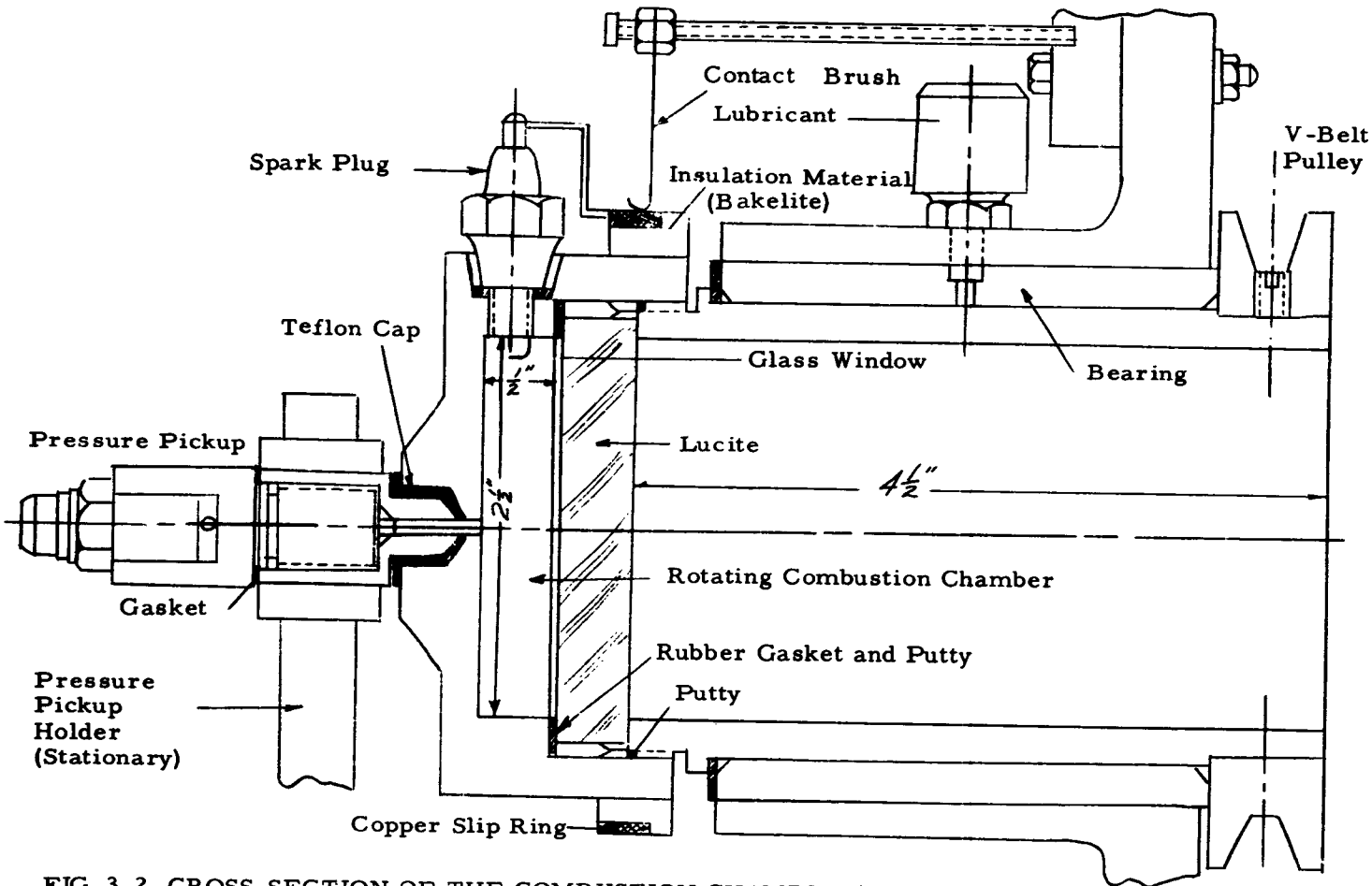

FIG. 3.2 CROSS-SECTION OF THE COMBUSTION CHAMBER (FULL SCALE).

the pressure pickup was located represented the chamber pressure.

The combustion chamber was threaded unto a hollow steel cylinder as shown in Fig. 3. 2. The hollow cylinder was supported by a journal bearing that was designed for a main bearing of a G. M. C. automobile crankshaft. Since the operating time for the combustion chamber was only a few minutes, the journal bearing was lubricated by use of a gravity lubricator with SAE 30 engine oil. Thus the hollow cylinder provided a rotational mounting for the combustion chamber. A V-groove on the hollow cylinder was belted to a variable speed drive driven by an electric motor. The cylinder with the combustion chamber attached could thus be driven at speeds from 0 to 3600 rpm.

Spark Plug:

The spark plugs used were AC type M-8 (Fig. 3. 3). The active spark plug was connected to a copper ring supported by a Bakelite ring mounted on the outside of the combustion chamber. This ring provided an electrical connection from the induction coil (Fig. 3. 1 and 3. 2) to the rotating chamber. The electrode of the active spark plug was modified with copper wires of different lengths to provide for ignition at three points in the cylindrical chamber--at the periphery, point of half radius from the center, and at the center.

Pressure Pickup:

The pressure was measured using a piezoelectric pickup with a range of 0 to 1000 psi, electrically connected to a Model 533 Tektronix oscilloscope through a calibrator. The diaphragm

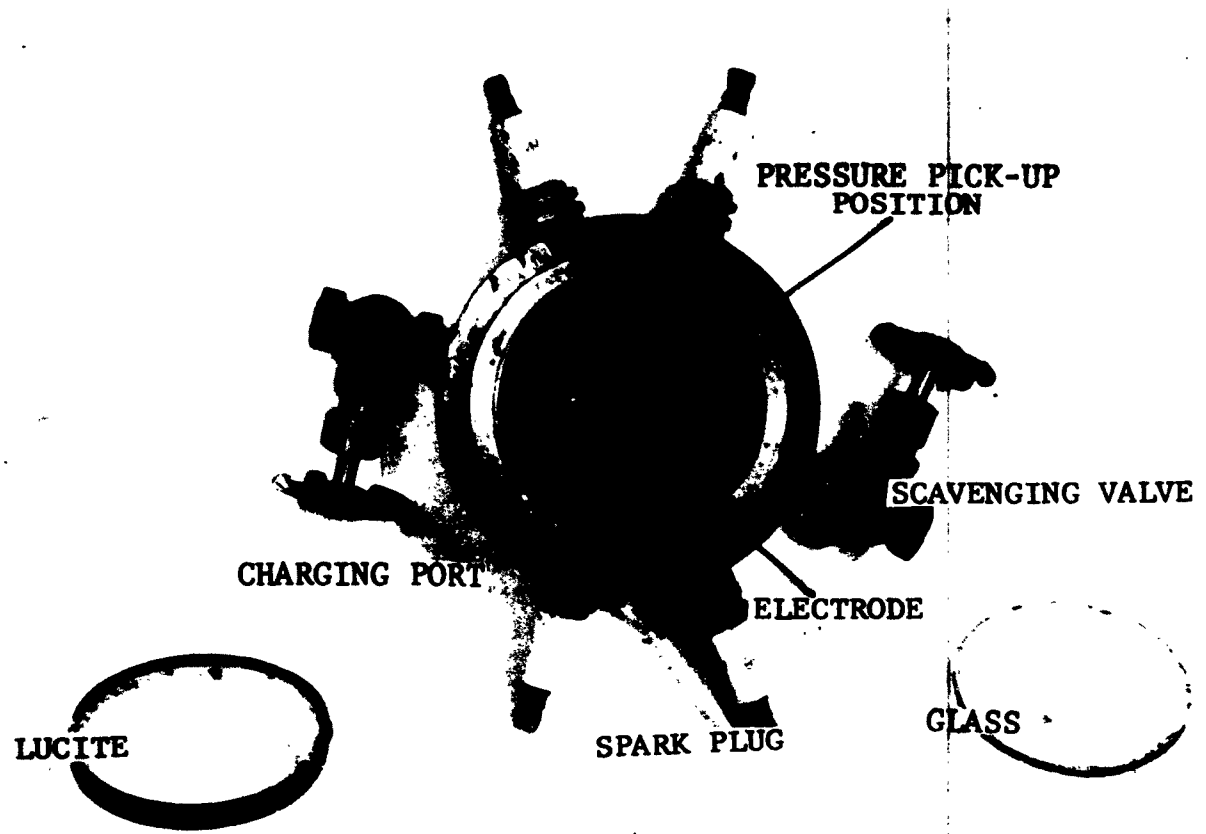

FIG. 3•3. COMBUSTION CHAMBER

end of the pressure pickup was threaded into an adaptor which was supported by the holder as shown in Fig. 3. 2. Thus the pressure pickup was stationary, and as noted, the combustion chamber was rotatable. To prevent leakage around the contact surface between the pressure pickup adaptor and the combustion chamber, a Teflon cap was attached to the adaptor with epoxy cement. This provided an essentially leak free bearing surface between the pressure pickup and the rotative combustion chamber, with force applied from the pressure pickup holder.

Driving Motor:

An A-C induction motor with a variable speed drive was connected by a single V-belt to the combustion chamber as shown in Fig. 3. 1. This motor was rated 1/2 hp, 1760 rpm, 222 volts, single phase.

Premixing Tank:

In parts (a) and (c) of Phase I, methane was used to determine the effect of rotative combustion chamber speed and location of the point of ignition on combustion time and maximum combustion pressure. (As noted later, acetylene was used to determine the flame trajectory.)

Before the methane-air mixture was charged to the combustion chamber, the methane and air were introduced to a premixing tank where they could become mixed homogeneously. The mixture ratio of methane to air could also be controlled in this tank. The premixing tank was made of plastic with 1/2 inch

scale markings on the surface. The diameter of the tank was 6 inches and the height was 7.5 inches. Thus, the volume of gas charged to the combustion chamber was determined by measuring on the scale markings the displaced water in the premixing tank. The accuracy of controlling the mixture ratio in this manner was adequate for the purpose of these tests.

In the determination of the flame trajectory with acetylene, the weight of the actylene-air mixture had to be more precisely measured, since the flame propagation speed of the acetylene-air mixture is very sensitive to variations of the mixture ratio (14). Therefore, the premixing tank was changed to a steel tank (of 21 cubic inch volume) which was connected to a 77 inch manometer by a 1/4 inch copper tube. More precise measurements of mixture ratios were possible with the manometer. This steel premixing tank was also used for the nonhomogeneous mixture combustion tests.

3.1.2 Photographic Equipment

As shown in Fig. 3.1 the oscilloscope was connected to the piezocalibrator as an indicator to show the pressure variation during combustion. A Polaroid camera, using Polaroid Type 42 film, was attached to the oscilloscope in order to make a permanent record of the measurements of pressure variation. The oscilloscope was intensity modulated from a time mark generator to give an accurate time reference on the photographs.

High speed photographs of the flame during combustion were made through the Lucite and glass window on the end of the

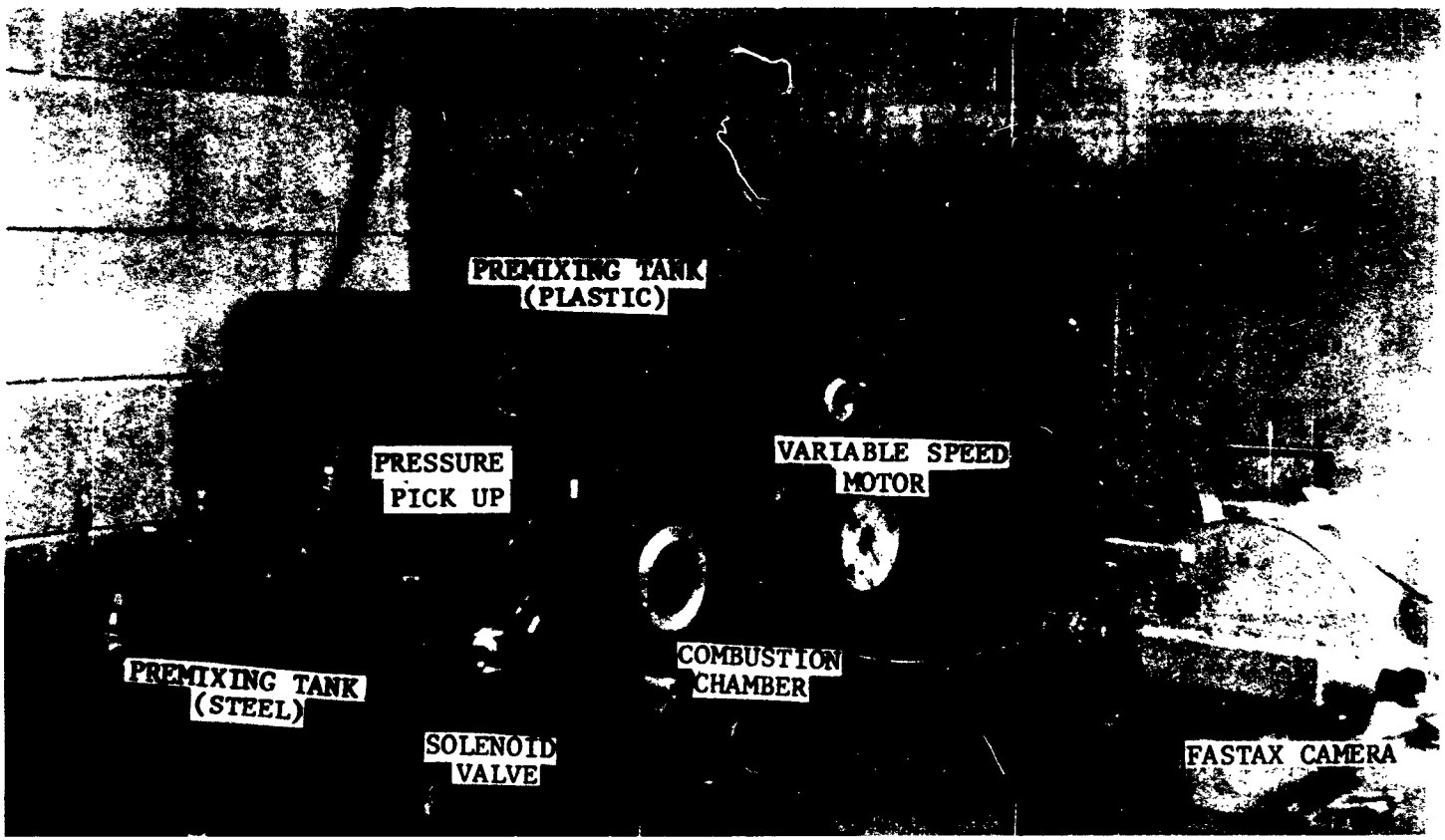

FIG. 3.4. THE EXPERIMENTAL SET UP.

combustion chamber in order to determine experimentally the flame trajectory and in order to observe flame spread. These photographs were taken with a 16mm Fastax camera, with its lens located 28 inches from the center of the combustion chamber and the aperture fully open. As noted in Fig. 3.1 and 3.4, the photographs were taken through the center of the hollow steel cylinder supporting the combustion chamber. Since the combustion time was of the order of 10 milliseconds, only about 25 feet of Kodak Tri-x film was used for each record. This camera produced a 1/120 second time mark on the film so that an accurate time scale could be obtained for the flame trajectory photographs, independent of the small variations in the camera speed.

3.1.3 Electrical System:

Since this investigation was to determine the various effects during combustion time, and since the physical phenomena occur during a period of about 5 to 10 milliseconds, an electric recording system, synchronized with the normal electrical ignition system, was necessary.

The ignition system and the recording system are shown in schematic form in Fig. 3.5. The ignition system consisted of a 6 volt battery, switches S1 and S2, solenoid relay, an induction coil, and a spark plug. The recording system consisted of the piezo-calibrator, Tektronix type 181 time mark generator, audio frequency amplifier, and Tektronix oscilloscope type 533. The time mark generator produced 1 millisecond time marks by intensity modulation of the oscilloscope.

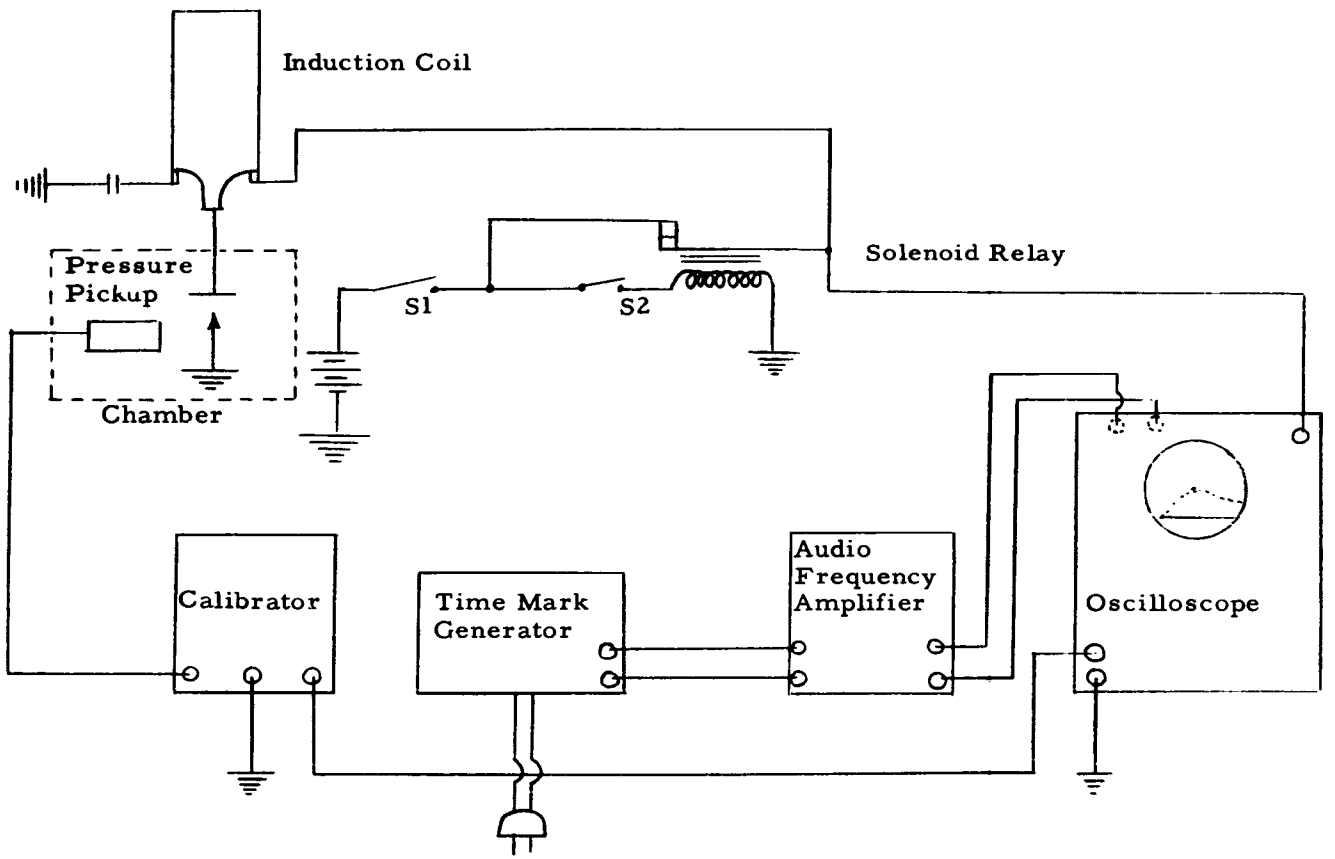

FIG. 3.5. WIRING DIAGRAM FOR EXPERIMENTAL SETUP.

The piezocalibrator provided a calibration voltage so that the vertical deflection of the oscilloscope could be accurately calibrated in psi to the signal from the piezoelectric pickup.

The type 533 Tektronix oscilloscope has a rise time of 0.025 microseconds, which is more than adequate to record accurately the pressure variations which occurred during the 10 millisecond combustion time.

3.1.4 Experimental Procedure:

In parts (a) and (c) of Phase I, methane gas was used to determine the effect of the combustion chamber rotative speed and location of the point of ignition on the combustion time and chamber pressure. Methane gas was introduced into the premixing tanks and measured by the volume of water displaced. Air was then introduced into the premixing tank until the methane to air ratio was 1:10 in volume. In order to insure a homogeneous mixture of air and methane, the mixture was kept in the premixing tank for a few minutes.

The combustion chamber was scavenged by the methane-air mixture, and then a charge of the methane-air mixture was introduced into the combustion chamber. The volume of the mixture charged was three times that of the chamber volume at atmospheric pressure. The volume of the charge was measured by the scale marked on the surface of the premixing tank.

During the test with methane, it was discovered that the color of the methane flame was unsuited to the photographic recording of the flame trajectory. Also, the ratio of the density

of the air to that of the burning methane-air mixture flame is unknown, but this ratio was needed to calculate the flame trajectory as shown by Equation 2.9 and 2.10. The acetylene-air mixture with a few drops of aniline added proved to give quite satisfactory flame photographs; and the density ratio of an air to acetylene-air mixture flame is known to be approximately 3.0. Therefore, in parts (b) and (d) of Phase I, acetylene was substituted in order to obtain all needed data in connection with the flame trajectories.

As noted in Section 3.1.1, the steel mixing tank with the 77 inch manometer for more precise measurements was used for the acetylene. This premixing tank, with air at atmospheric pressure, was then charged with acetylene gas to a pressure of 19 inches of mercury above atmospheric pressure. This resulted in an acetylene to air mixture ratio of 1: 1.74 in weight. This mixture was allowed to remain in the tank until the air remaining in the mixing tank could be assumed to have mixed homogeneously with the acetylene. After scavenging the combustion chamber with air, the acetylene-air mixture was then charged into the combustion chamber from the premixing tank through the inlet valve (1/8 inch pipe needle valve) until the pressure in the premixing tank decreased by 1.5 inches of mercury (0.316×10^{-4} lb).

During all tests in Phase I, before ignition was effected, the A-C motor with the variable speed drive was switched on and the speed of the combustion chamber was held constant for one or two minutes in order to ensure that the gas mixture within the combustion chamber attained a constant speed of solid body

rotation on one hand (7) and that the fuel-air mixture became mixed homogeneously on the other hand. Next, switch S1 was turned on for a few seconds to excite the induction coil, the shutter of the Polaroid camera was opened, the Fastax camera and switch S2 were turned on. Upon completion of the above procedure, at the end of combustion, the shutter of the Polaroid camera was closed. Figure 3.6 shows the flow diagram of this procedure. When switch S1 is turned on, the induction coil is energized. When switch S2 is turned on, the solenoid relay is opened and the secondary of the induction coil is brought to a high voltage which causes the spark in the combustion chamber. This high ignition voltage also initiates the horizontal sweep on the oscilloscope through the triggering input and produces a spike on the oscilloscope trace. The Polaroid camera photographed this spike, which established the beginning of combustion. Since the trace on the oscilloscope was also marked with 1 millisecond time marks, the relationship between combustion pressure and time and total combustion time was easily found.

Since the combustion chamber was small, combustion pressure in the entire chamber was assumed to be uniform. Therefore the curve of the relationship between combustion pressure and time, which was recorded by the Polaroid camera, may be assumed to represent the relationship between the combustion pressure and time for the entire combustion chamber.

Following the procedure described above, the effect of the rotative chamber speed and location of the point of ignition

Note. Circled Numbers Indicate The Order of Operation.

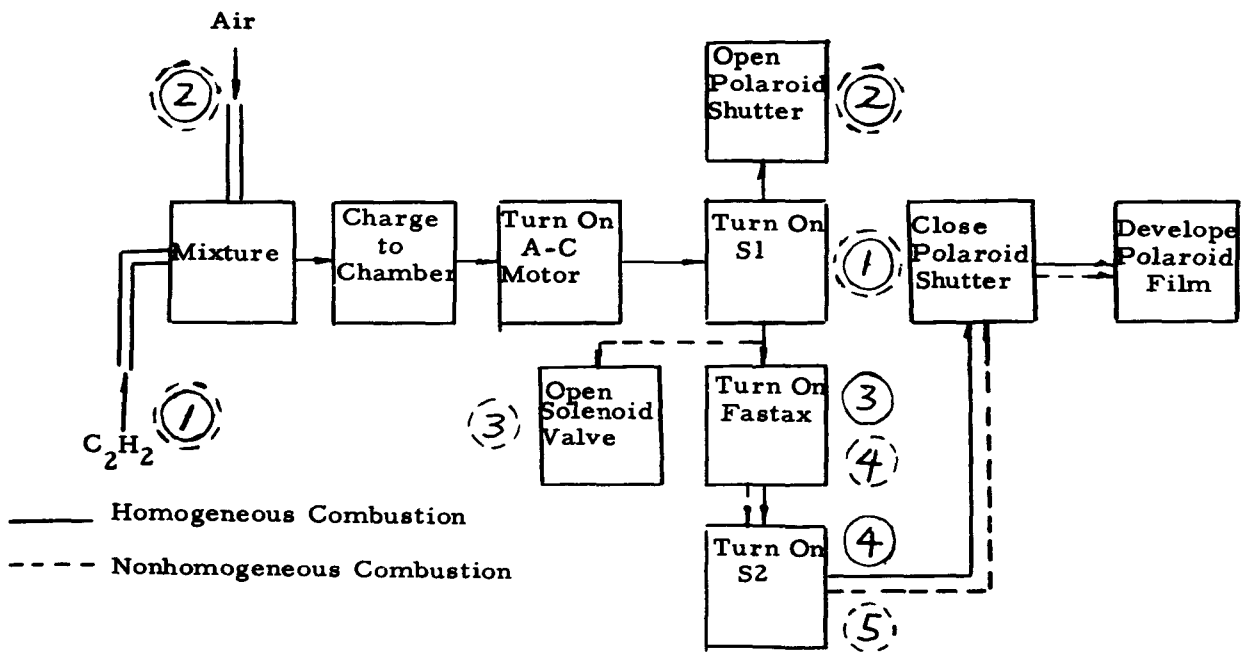

FIG. 3.6. FLOW DIAGRAM OF EXPERIMENTAL PROCEDURE

on combustion time and maximum combustion pressure were made at rotative combustion chamber speeds of 0, 500, 900, 1350, 1800, 2700 and 3600 rpm. Throughout the experiments, the combustion chamber was charged with a methane-air mixture of three times the volume of the chamber, and a constant methane-air mixture ratio of 1:10 was maintained.

For part (d) of Phase I, in the experimental determination of flame trajectories, observations were made at the rotative combustion chamber speed of 900 and 1800 rpm with ignition taking place at a point of half radius from the center. An acetylene-air mixture with a mixture ratio of 1:1.74 and an amount of 0.316×10^{-4} lb was used throughout the tests.

3.1.5 Flame Photography:

The flame color of the methane gas mixture is blue at any mixture ratio, and is rather difficult to photograph. Therefore as noted before, an acetylene mixture was used for the experimental determination of the flame trajectory because it gave a red color flame at a rich mixture ratio, thus allowing sufficient light for film exposure. Carbon particles which were deposited on the glass window as a result of combustion were removed after each experiment. Even with acetylene, a lean mixture ratio resulted in a red/blue flame which was difficult to photograph. To obtain better flame photographs in this case, it was necessary to intensify the color of the flame. For this purpose, a catalyst, aniline ($C_6H_5CN_2$), was used. Aniline contains a CN radical which, when burning, emits an orange color which is strong enough to record

on Kodak Tri-x film. In order to achieve a homogeneous mixture, a few drops of aniline were added to the acetylene-air mixture in the steel premixing tank, thus allowing evaporated aniline to mix with the fuel mixture. Other catalysts which could have been used are metyl amine (CH_3NH_2), metyl nitrate (CH_3NO_3), or nitrobenzen ($C_6H_5NO_2$). Of these, only nitrobenzen was tried, but it was found that aniline gave better results. Since aniline is very toxic it was necessary to avoid inhaling the fumes.

3.2 Apparatus and Experimental Procedure for Phase II.

In Phase II of the investigation the premixing steel tank, the ignition system, and recording system were the same as those used in Phase I. In this section the modified combustion chamber, fuel charging system, and the necessary photographic technique will be described. An attempt has been made to develop an empirical method of predicting the effect of the combustion chamber rotative speed and location of the point of ignition on the combustion time for the nonhomogeneous mixture combustion.

3.2.1 Modified Combustion Chamber and Charging System

In order to produce a nonhomogeneous mixture in the combustion chamber, the chamber was modified to simulate the conditions of a diesel engine. The combustion chamber was modified as shown in Fig. 3.7. The modification was made only on the pressure pickup side to provide a means of charging the combustion chamber while it was being rotated. A small copper tube 1/16 inch in diameter was connected directly to the diaphragm side of the pressure pickup through the adaptor utilizing the

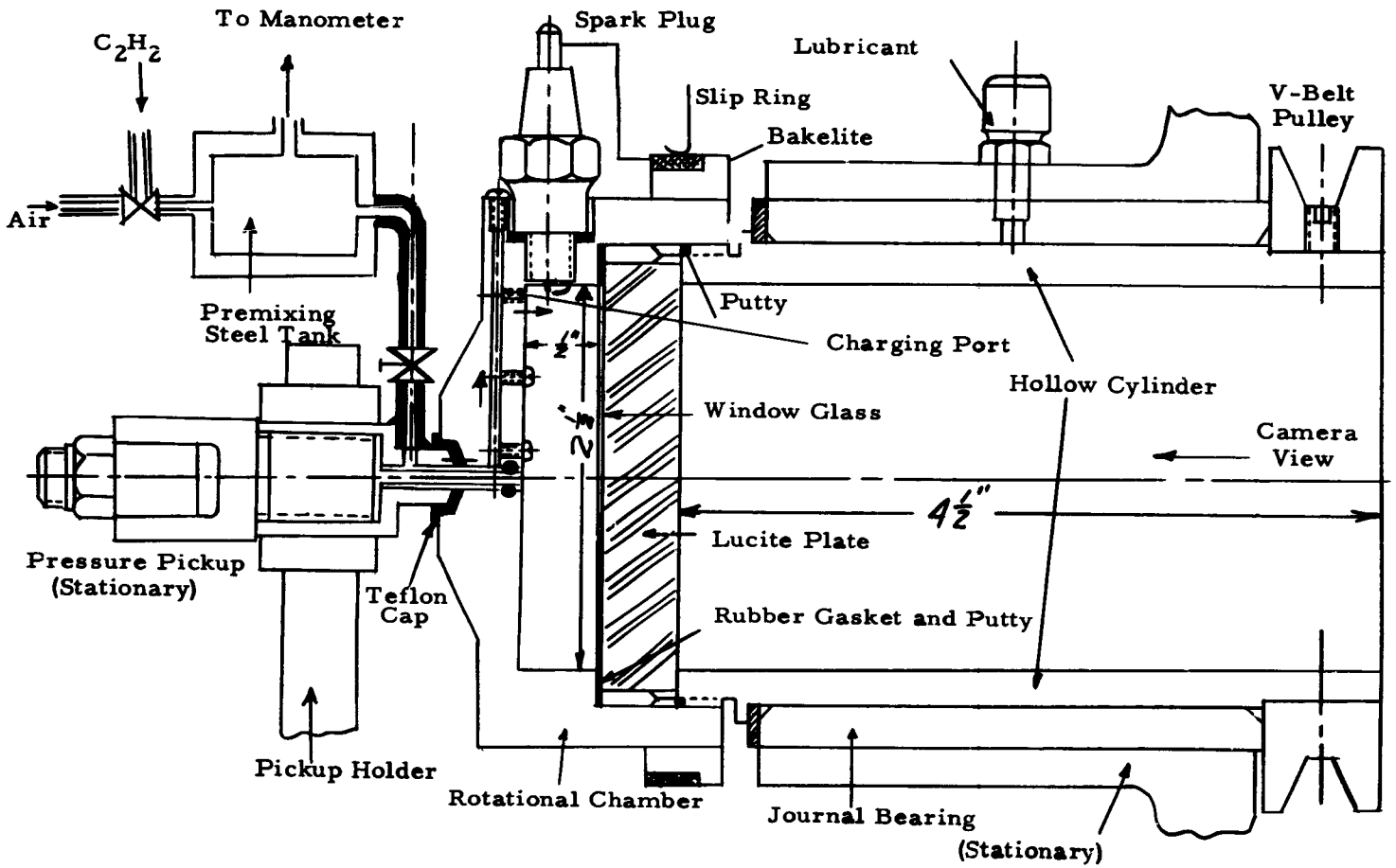

FIG. 3. 7. MODIFIED COMBUSTION CHAMBER (FULL SCALE)

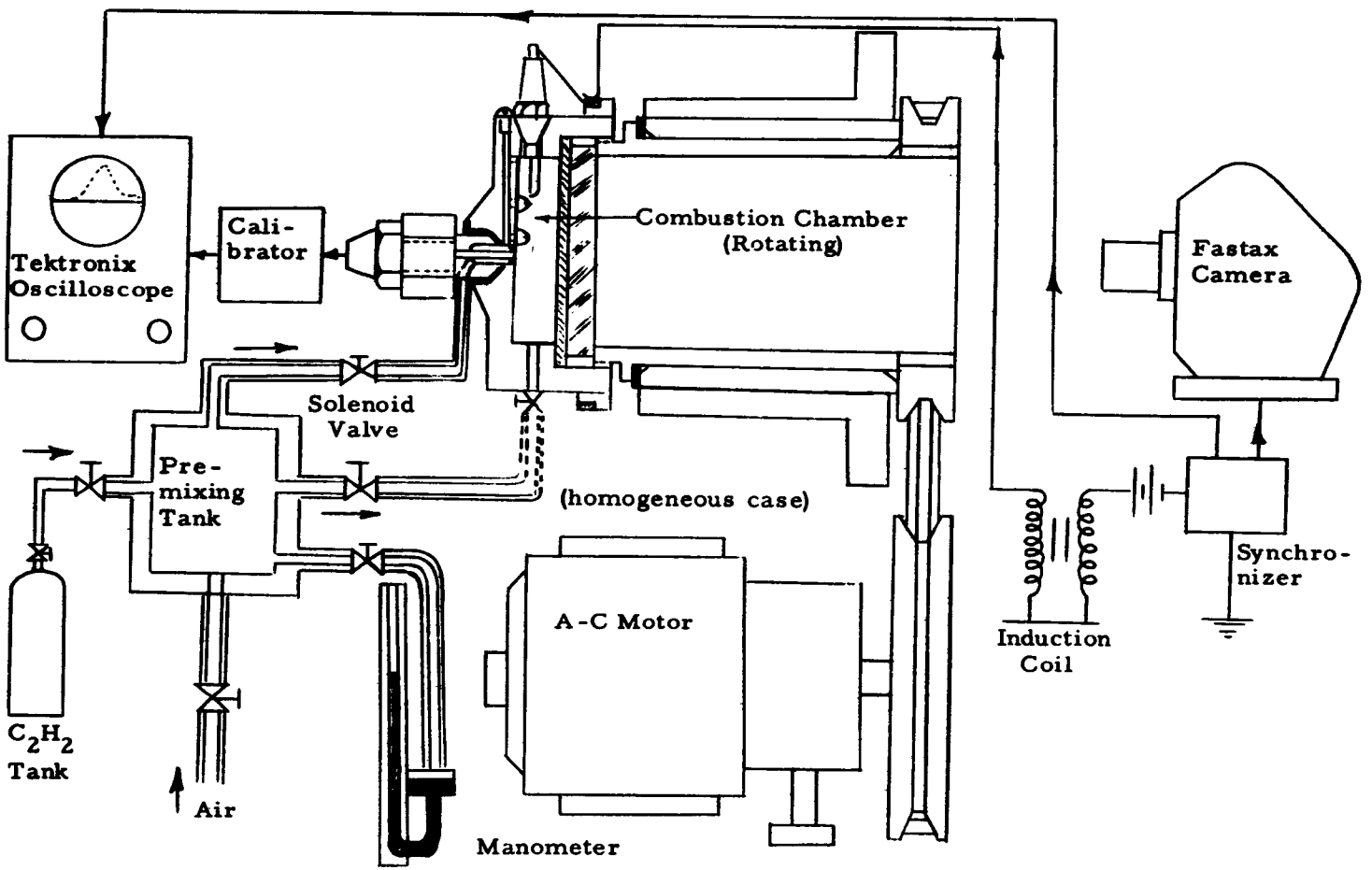

FIG. 3.8. EXPERIMENTAL SETUP FOR NONHOMOGENEOUS MIXTURE COMBUSTION.

clearance around the tube as an inlet passage into charging ports drilled in the chamber cover. Charging ports were made at the periphery, half radius from the center, and the center of the combustion chamber. The desired charging port was left open while the other two were closed during an experiment. The location of the point of ignition was also changed to one of the three positions (periphery, half radius from the center, or center) for each of the charging locations. This modification enabled the observation of flame spread to be made with any combination of rotative combustion chamber speed, location of charging port, and location of the point of ignition.

In the case of the flame trajectory measurements it was necessary to synchronize the charging of the fuel to the combustion chamber with the ignition and recording events. This need for synchronizing is due to the fact that it is desirable, as explained in 5.2, to ignite the flammable mixture while it is still contained within the restricted region around the charging port, instead of having it spread throughout the chamber. A solenoid valve was inserted in the line between the steel premixing tank and modified combustion chamber to accomplish this synchronization.

3.2.2 Experimental Procedure:

In order to find the effects of the combustion chamber rotative speed, location of the point of ignition, and charging port position on combustion time and on the flame trajectory for the nonhomogeneous mixture combustion, parts (f), (g), and (h), the

modified combustion chamber and charging system were used. An overrich acetylene-air mixture was used in this part of the nonhomogeneous mixture combustion tests.

The acetylene gas was charged into the steel premixing tank until the pressure was 10 inches of mercury above atmospheric. Then air was charged to the tank until the absolute pressure was 43.92 inches of mercury above atmospheric (the acetylene-air mixture ratio was 1:4.85 in weight). When the combustion chamber reached the desired speed, the acetylene-air mixture was charged into the chamber through the desired charging port (refer to Fig. 3.7 and 3.8) until the pressure in the premixing tank decreased to 1 inch of mercury (0.3×10^{-4} lb in weight). In the investigation of the variation in combustion time, parts (f) and (g), it is necessary to have the mixture ignited soon after the charging. However, there is no need to achieve such a critical synchronization between the charging of the mixture and the ignition as necessary in the study of flame trajectories, part (h), since the condition of nonhomogeneity of the mixture persists in the chamber for a reasonable period of time. Therefore no attempt was made to synchronize the charging with ignition and recording for the measurements in parts (f) and (g). The charging valve used was a 1/4 inch pipe needle valve, hand operated. The firing and recording procedures were the same as outlined in Section 3.1.3.

In the experimental determination of the flame trajectory it was necessary to control accurately the quantity of the fuel charged to the combustion chamber, and to synchronize the ignition

with fuel charging and the recording events. The synchronization was accomplished by the use of the solenoid valve. However, since the pressure at the charging port changed with combustion chamber speed, the amount of gas mixture entering the chamber when the solenoid valve was opened varied depending on the combustion chamber rotative speed and thus made it rather difficult to control the amount of mixed fuel that was charged.

It was experimentally determined that, when acetylene was charged into the steel premixing tank which was originally filled with air to a pressure of 3 inches of mercury, an acetylene-air mixture with a mixture ratio of 1:11 resulted in the tank. Furthermore, when the solenoid valve was opened to charge the mixture into the combustion chamber which was rotating at 900 rpm, the pressure in the tank was allowed to decrease by 0.3 inch of mercury, indicating that 0.09×10^{-4} pounds of mixture had been charged into the chamber.

In view of such a lean mixture in the combustion chamber, it was necessary to intensify the brightness of the flame for flame photography by adding a few drops of aniline to the steel premixing tank as noted previously in Section 3.1.4. After the combustion chamber obtained a speed of 900 rpm, switch S1 (refer to Figures 3.5 and 3.6) was turned on and the shutter of the Polaroid camera was opened. The solenoid valve, the Fastax camera, and switch S2 were turned on simultaneously (refer to Figures 3.5 and 3.6). After combustion was completed, the shutter of the Polaroid camera was closed.

As in Phase I for the homogeneous case and using the same procedure, photographic recordings were taken of the combustion pressure as a function of time on the oscilloscope with the Polaroid camera and of the flame itself with the Fastax camera. The results of the experimental work are described in Chapter IV.

IV. RESULTS OF EXPERIMENT AND THEORETICAL CALCULATION

4.1 Results of Preliminary Tests

Two preliminary tests were carried out for the purpose of observing the general behavior of the combustion pressure variation and the development of flame during combustions.

For the first test part (a) of Phase I, a flammable mixture of methane gas and air with a relatively slow burning velocity was used. Combustion pressure variations were obtained and compared for chamber rotative speeds of 1800 and 2700 rpm when the mixture was ignited at the periphery of the chamber. These results are summarized in Fig. 4.1, from which it can be seen that the maximum combustion pressure remained reasonably constant in spite of the fact that the combustion time varied. Variation in combustion time is very large at 2,700 rpm as indicated in Fig. 4.1. This is believed to have been caused by vibration of the combustion chamber. During the experiments the chamber was frequently observed to resonate around 2,700 rpm.

For the second test, part (b) of Phase I, a Fastax high speed camera was used in order to photograph the flame development under the influence of centrifugal and drag forces. High speed pictures of the flame were taken using a rich acetylene-air mixture, which burns with high flame luminescense. It was observed that at high chamber rotative speeds the flame, when ignited at the periphery of the chamber, moved radially inward describing a spiral curve. Afterward, the flame moved outward from the center until the entire chamber was filled with the flame.

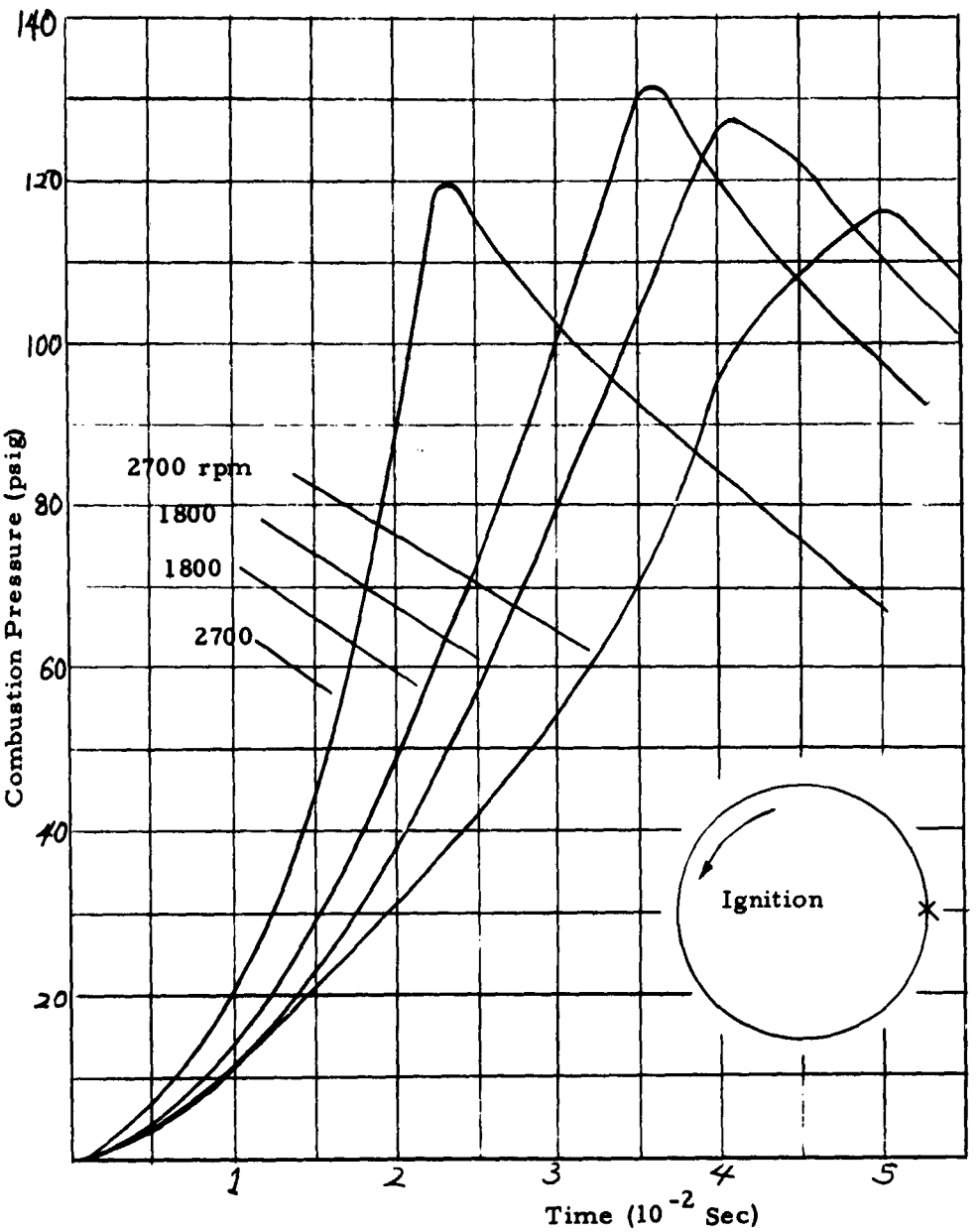

FIG. 4. 1. CHAMBER PRESSURE VS. COMBUSTION TIME FOR VARIOUS ROTATIVE CHAMBER SPEED FOR THE HOMOGENEOUS MIXTURE COMBUSTION.

It is noteworthy that a pair of appreciably strong swirls of opposite sense resulted as the flame disappeared, as shown in Fig. 4.2 and Fig. 4.3. In the static chamber the flame propagation is observed to have the shape shown in Fig. 4.4.

4.2 Results of the Effect of Location of the Point of Ignition and Chamber Rotative Speed on Combustion Time for Homogeneous Mixture Combustion.

The combustion times were compared for combustion chamber rotative speeds of 0, 500, 900, 1300, 1800, 2700, and 3600 rpm and at three locations of the point of ignition: at the periphery, half radius from the center, and the center. Throughout the tests, the combustion chamber was charged with methane-air mixture as specified in Part (c) of Table 3.1. The results are summarized in Fig. 4.5.

In the case of ignition at the periphery, the influence of the combustion chamber rotative speed on the combustion time is most distinct. The combustion time at high speeds was approximately 40% lower than the combustion time for the stationary chamber.

In the case of ignition at the center, on the other hand, the combustion time was less influenced by the combustion chamber rotative speed. The combustion time was almost independent of the chamber speed.

4.3 Results of the Effect of Location of the Point of Ignition and Combustion Chamber Rotative Speed on Combustion Time for the Nonhomogeneous Mixture Combustion.

The effect of changes in the location of the point of ignition

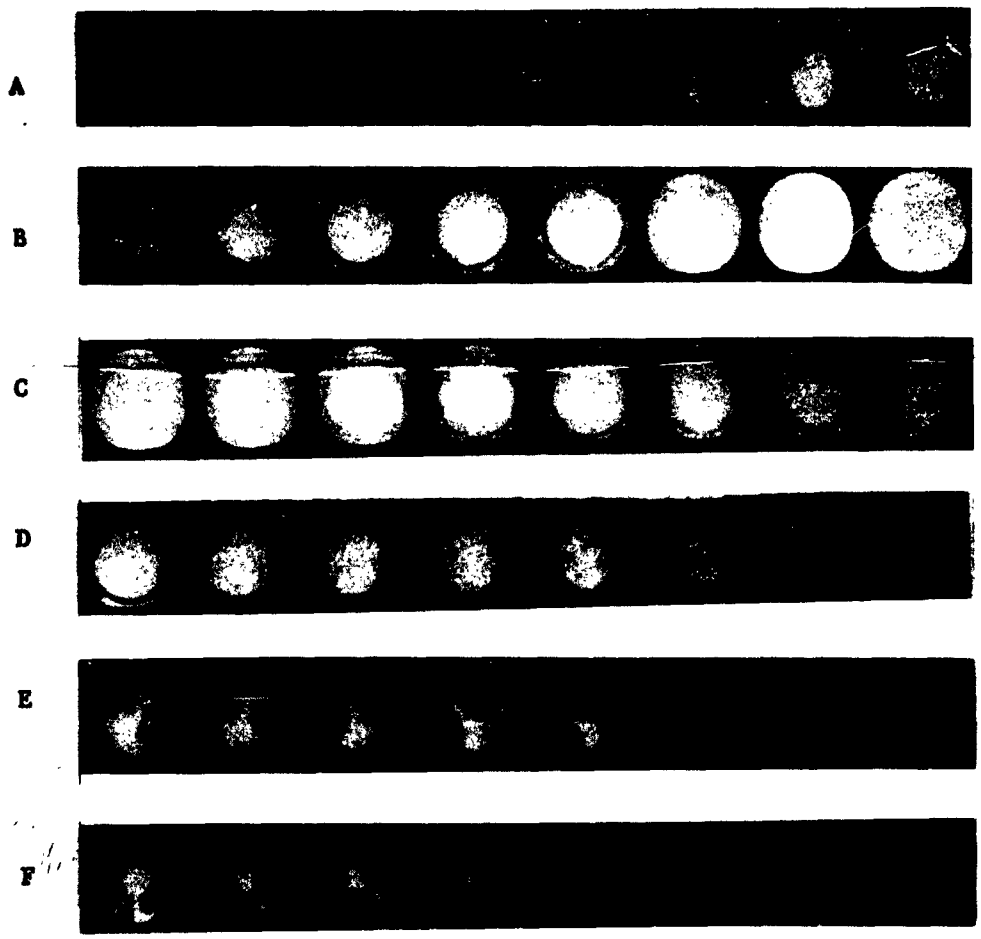

FIG. 4. 2 FLAME PATTERN IN HOMOGENEOUS MIXTURE COMBUSTION AT 2400 RPM.
4500 FRAMES PER SECOND
MIXTURE RATIO (ACETYLENE TO AIR) 1:7
(CONTINUOUS SINGLE FILM STRIP DISPLAYED IN SIX SECTIONS, A THROUGH F.)

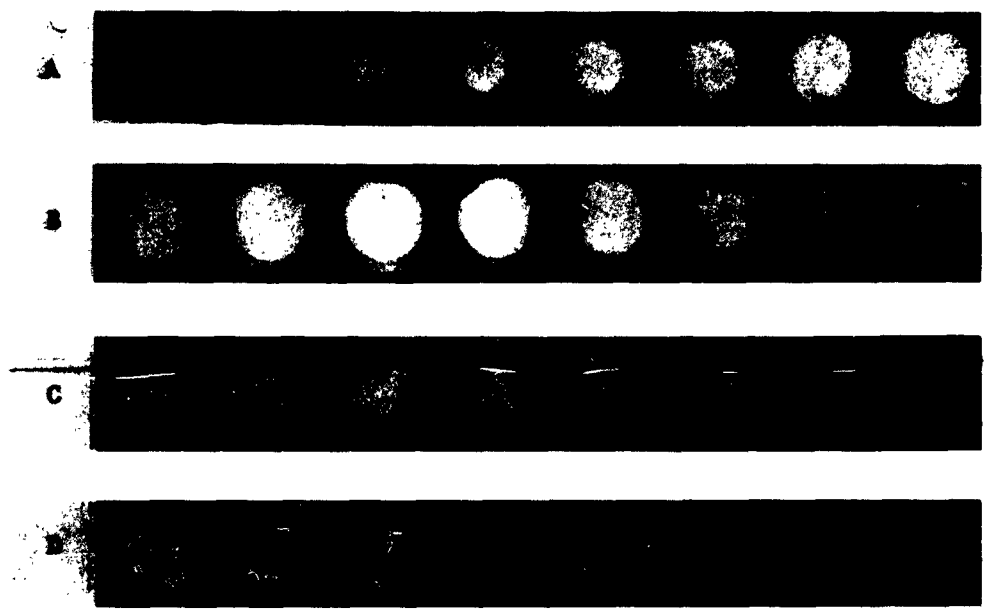

FIG. 4. 3. FLAME PATTERN IN HOMOGENEOUS MIXTURE COMBUSTION AT 2700 RPM.
4500 FRAMES PER SECOND.
MIXTURE RATIO (ACETYLENE TO AIR) 1:7
(CONTINUOUS SINGLE FILM STRIP DISPLAYED IN FOUR SECTIONS, A THROUGH D.)

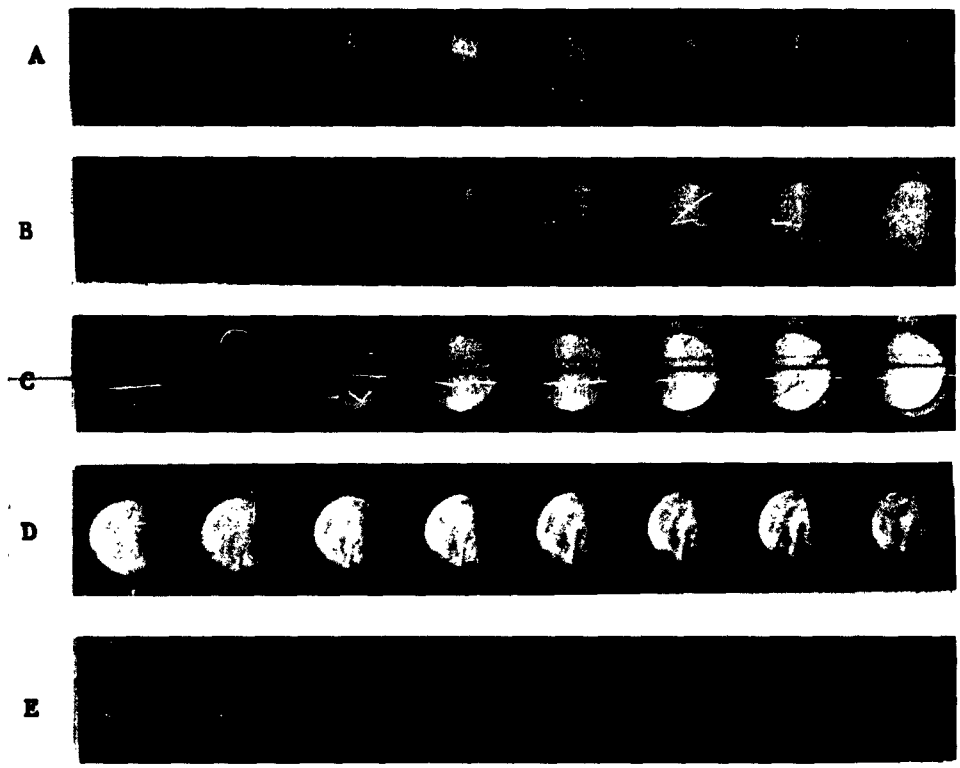

FIG. 4.4. FLAME PATTERN IN HOMOGENEOUS MIXTURE COMBUSTION AT STATIONARY.
4500 FRAMES PER SECOND.
MIXTURE RATIO (ACETYLENE TO AIR) 1:7
(CONTINUOUS SINGLE FILM STRIP DISPLAYED IN FIVE SECTIONS, A THROUGH E.)

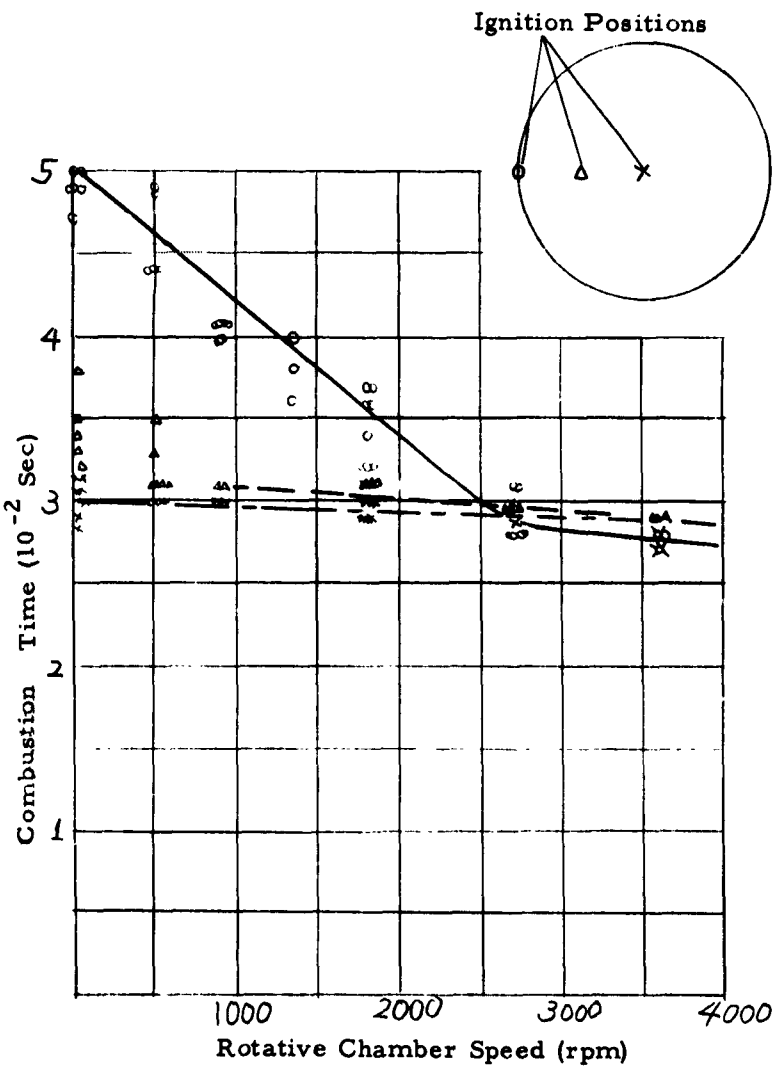

FIG. 4.5. COMBUSTION TIME VS. ROTATIVE CHAMBER SPEED FOR THE THREE IGNITION POSITIONS. (HOMOGENEOUS CASE).

and of the combustion chamber rotative speed on combustion time for the nonhomogeneous mixture combustion was investigated, using the apparatus shown in Fig. 3.7 and Fig. 3.8, for three locations of the point of ignition (periphery, half radius from the center, and center) and for two locations of the charging port, one at the periphery and the other at half radius from the center. Throughout these tests, an overrich acetylene-air mixture, as specified in Part (f) of Table 3.1, was admitted through the charging port. The results of these tests are shown in Fig. 4.6 and 4.7. Each point given in Fig. 4.6 and Fig. 4.7 represents the arithmetic mean value of four tests carried at each chamber rotative speed.

The experiment was first carried out using the charging port at the periphery. In the case of ignition at the periphery, the influence of combustion chamber rotative speed on the combustion time is evident in Fig. 4.6. The combustion time at high speeds was approximately 30% lower than the combustion time when the chamber was stationary. In the case of ignition at the center (refer to the description in 3.1.1), the combustion time was influenced little by combustion chamber rotative speeds; the combustion time at high speeds was approximately only 5% lower than that when the chamber was stationary.

In the second experiment of Part (f), the acetylene-air mixture was charged at a point of half radius from the center (refer to Fig. 3.7). and the three locations of the point of ignition (periphery, half radius from the center, and center) were used. As shown in Fig. 4.7, the combustion time increased slightly as

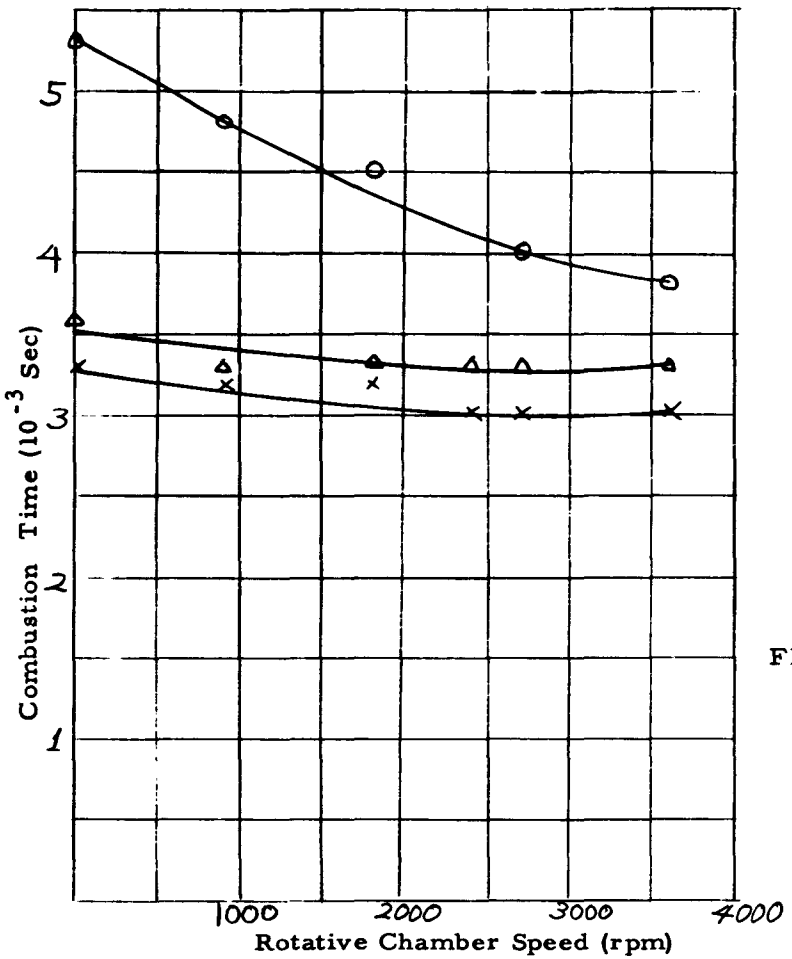

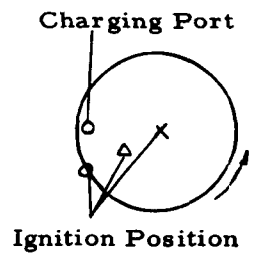

FIG. 4.6. COMBUSTION TIME VS. ROTATIVE CHAMBER SPEED FOR THE THREE IGNITION POSITIONS. (NONHOMOGENEOUS CASE)

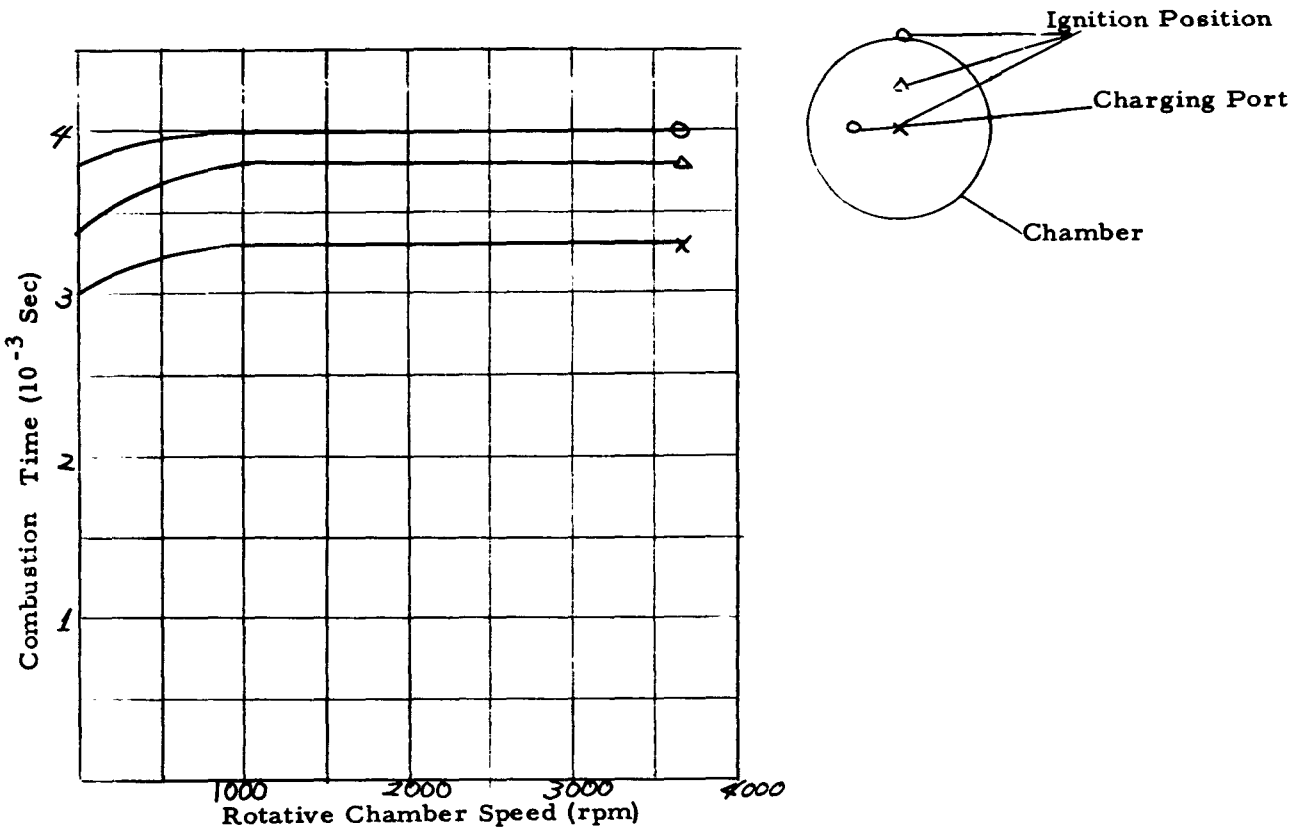

FIG. 4. 7. RELATIONSHIP BETWEEN COMBUSTION TIME AND ROTATIVE CHAMBER SPEED FOR CHARGING AT MIDCENTER.

the chamber speed increased for all three locations of the point of ignition. This increase in combustion time was about 5% of that when the chamber was stationary. When ignition was effected at each typical position (periphery, half radius from the center, and center), a pressure spike was recorded at the beginning of combustion on the photographs which were taken by the Polaroid camera. The reason for this photography will be discussed in Chapter V.

4.4 Comparison of the Effect of Combustion Chamber Rotative Speed on Combustion Time for Homogeneous and Non-homogeneous Mixture Combustion.

For the purpose of investigating the difference in the behavior of combustion in the homogeneous and nonhomogeneous mixture combustion cases, the effect of combustion chamber rotative speed on combustion time was studied for the two cases using overrich acetylene to air mixtures as specified in Part (e) and (g) of Table 3.1. The results shown in Fig. 4.8 indicate that the difference in the combustion time between the homogeneous and the nonhomogeneous mixture combustion is large.

4.5 Experimental Determination of Flame Trajectory.

In order to determine experimentally the flame trajectories and measure the flame radii, photographs were taken with the Fastax camera at 900 and 1800 rpm for the case of homogeneous mixture combustion with the ignition effected at half radius from the center of the combustion chamber. These

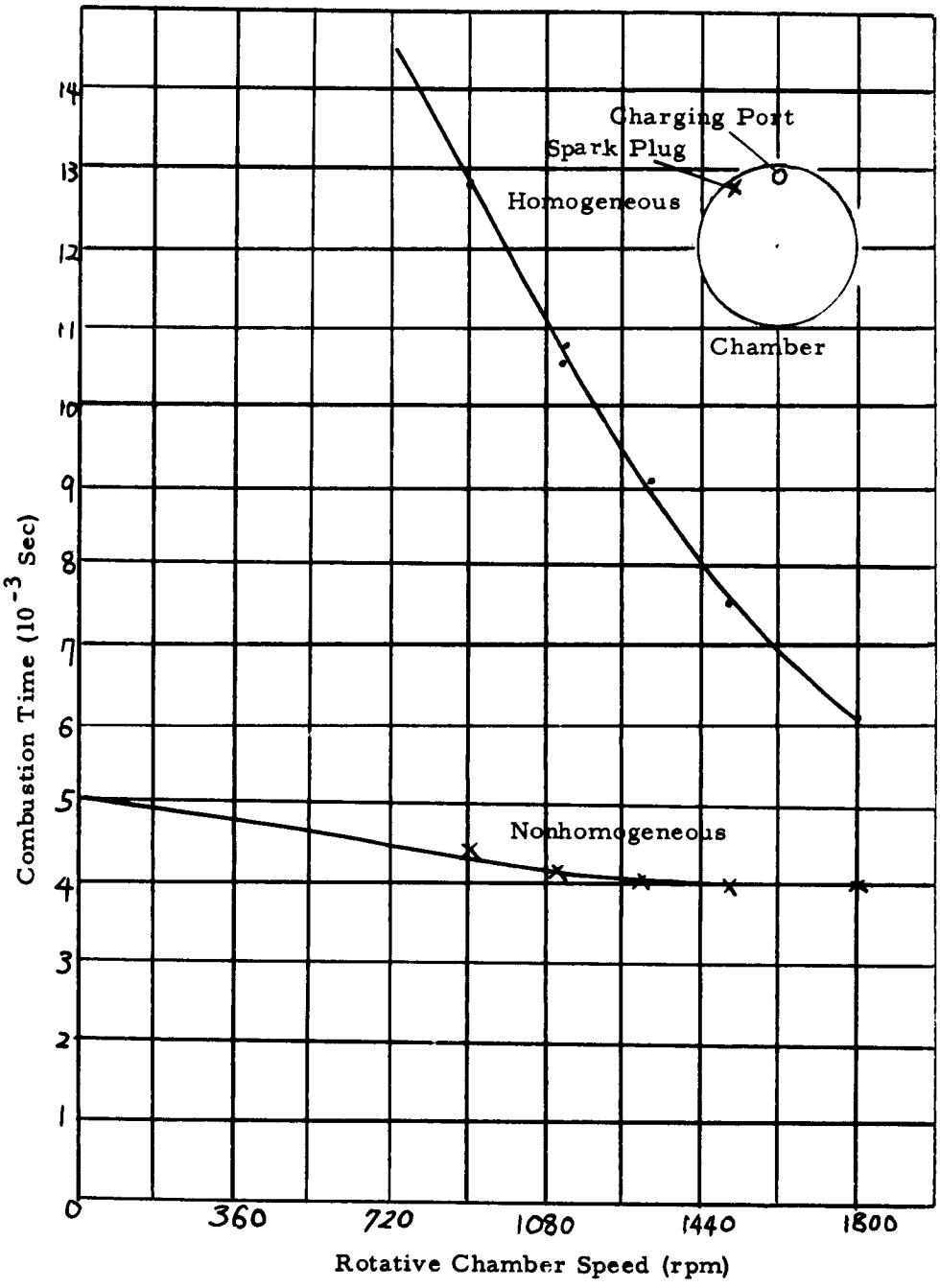

FIG. 4.8. COMPARISON OF COMBUSTION TIME FOR THE HOMOGENEOUS AND NONHOMOGENEOUS OVER-RICH MIXTURE.

pictures, which are shown in Fig. 4.9 and 4.10, were taken with the acetylene-air mixture as specified in Part (d) of Table 3.1.

For analysis these photographs were enlarged to 1.16 times actual size. The Fastax camera enabled the sparking point, that is the beginning point of combustion, to be photographed. From these photographs, which distinctly showed the outside contour of the combustion chamber, the center of the combustion chamber was also obtained.

It was rather difficult to determine the center of the flame because the flame did not form a perfect circle. It was therefore necessary to approximate such a circle by using the mean value of the maximum and minimum boundary of the flame front. After the flame made contact with the wall, the geometry of the flame deviated further from a circle. However, for the purpose of determining the center and the radius of the flame, the circle was approximated by the boundaries of the flame, although no attempt was made to consider analytically the development of the flame after it had made contact with the chamber wall.

Based on the position of the instantaneous centers of the flame thus determined, the flame trajectory could be obtained on a reference rectangular coordinate system, whose origin coincided with the geometrical center of the chamber, by expressing each flame center as a position vector originating from the center of the chamber. It was possible to superimpose

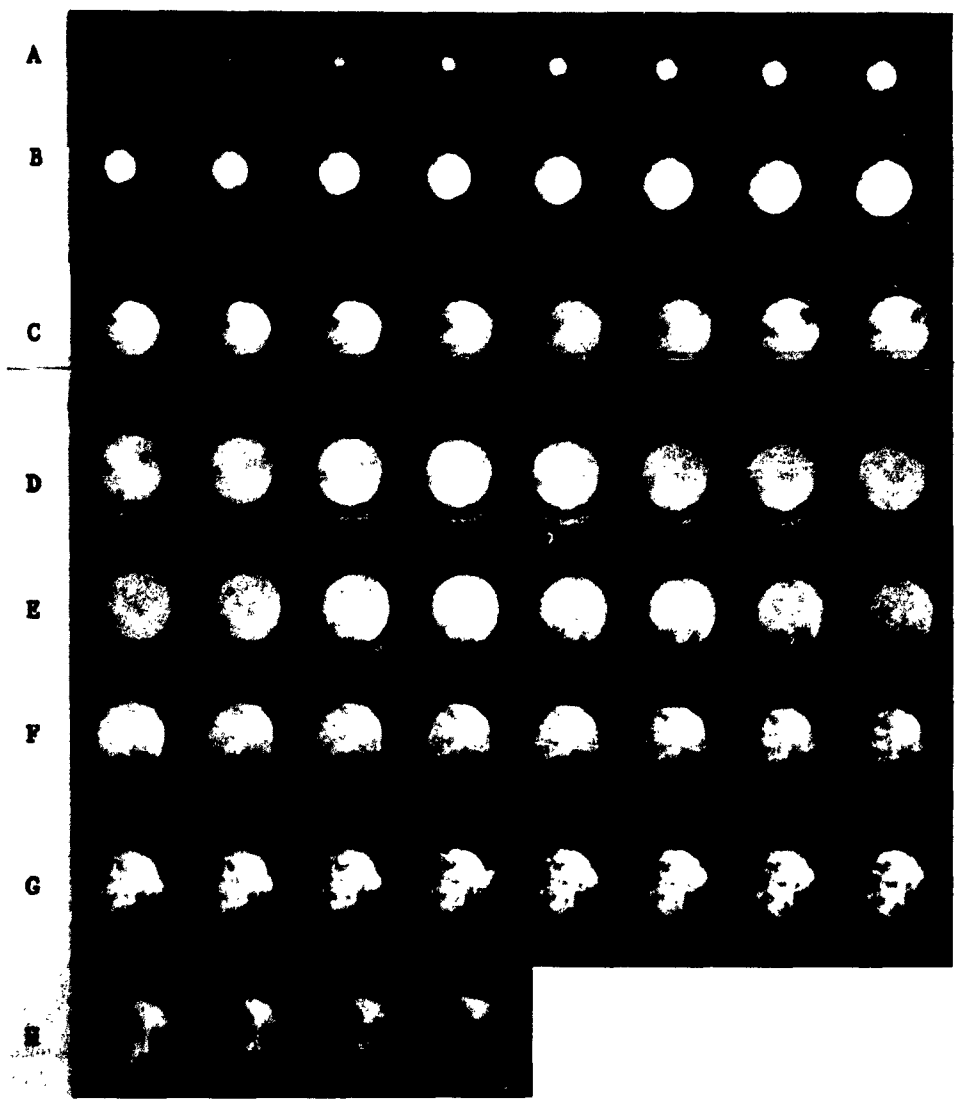

FIG. 4. 9. FLAME PATTERN USED FOR THE DETERMINATION OF FLAME TRAJECTORY BY EXPERIMENTAL METHOD AT 900 RPM. (3500 FRAMES PER SEC.) (CONTINUOUS SINGLE FILM STRIP DISPLAYED IN EIGHT SECTIONS, A THROUGH H.)

FIG. 4. 10 FLAME PATTERN WHICH WAS USED TO FIND FLAME TRAJECTORY BY EXPERIMENTAL METHOD AT 1,800 RPM. (3500 FRAMES PER SEC.) (CONTINUOUS SINGLE FILM STRIP DISPLAYED IN FOUR SECTIONS, A THROUGH D.)

the reference coordinate system on each frame of the film identically by making use of the perforation at the four corners of each frame. Judging from the extent of distortion in the circular shape of the flame shown in Fig. 4. 9 and Fig. 4. 10, it is believed that the flame made contact with the chamber wall at the time represented by the frames of Row B Column 7 and Row A Column 4 respectively. The triangular marks in Fig. 4. 11 represent the position of flame centers observed on every other frame of film or at intervals of 1. 1 milliseconds. The triangular marks in Fig. 4. 12 represent the position of flame centers observed on every frame of film, or at 0. 64 millisecond intervals at the camera speed used here. The measured data of the flame radius for both speeds of combustion chamber rotation are given in Fig. 4. 13. The data were obtained for the period before the flame made contact with the chamber wall.

Photographs were also taken for the nonhomogeneous case at a chamber speed of 900 rpm with both the mixture charged and ignition effected at half radius from the center of the chamber. These photographs are shown in Fig. 4. 14. As can be seen in this figure, a circular flame pattern did not develop.

4. 6 Results of Theoretical Calculations

As noted in Equation 2. 9 and 2. 10 given in Section 2. 3, the radius of the flame and the value of $\frac{\rho_a D}{\mu}$ as a function of time must be known in order to calculate the flame trajectory.

Since both the radius of the flame and the combustion pressure are functions of time, it should be possible to determine

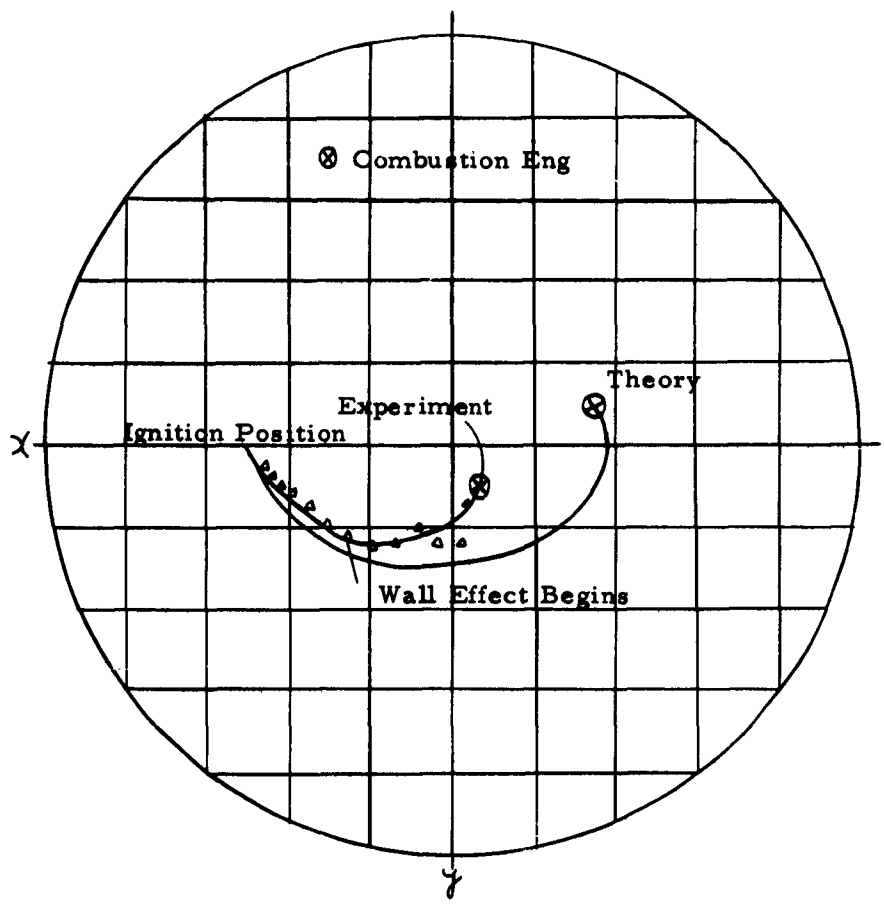

FIG. 4.11. COMPARISON OF THEORETICAL AND EXPERIMENTAL FLAME TRAJECTORIES AT 900 RPM.

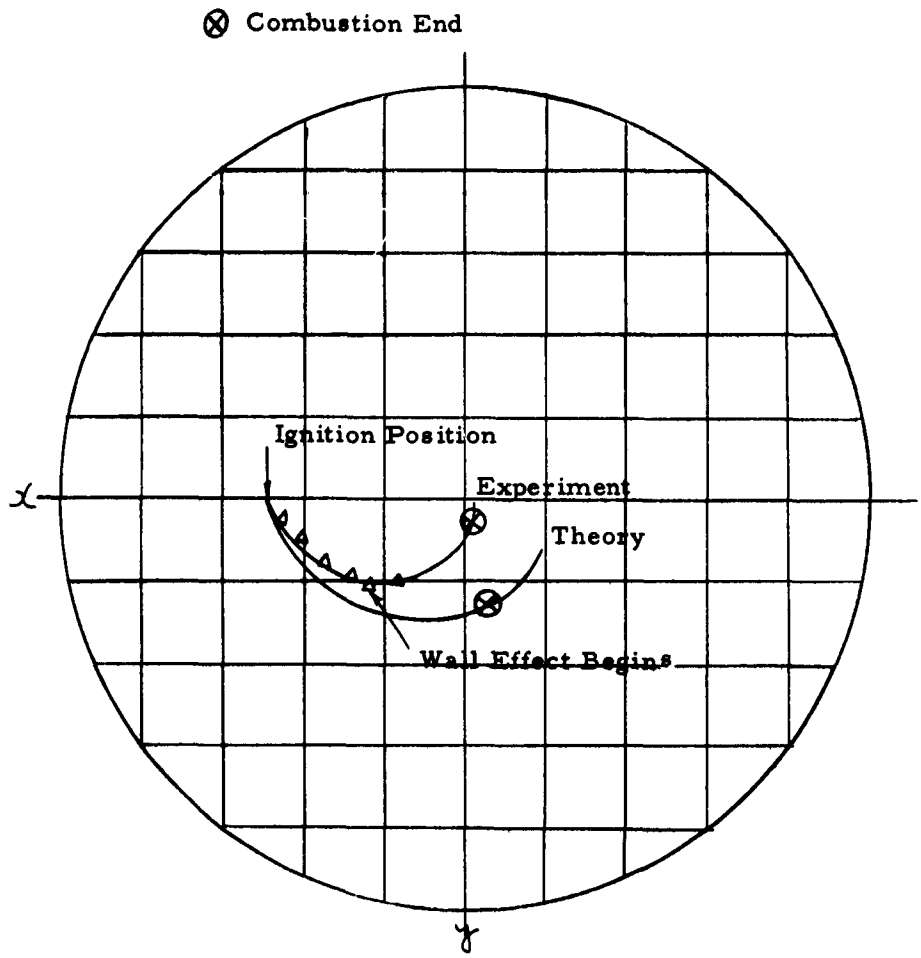

FIG. 4.12. COMPARISON OF THEORETICAL AND EXPERIMENTAL FLAME TRAJECTORIES AT 1800 RPM.

the relationship between the radius of the flame and the combustion pressure. However, the functional form of neither the radius of the flame nor the combustion pressure as a function of time is known as yet. Therefore, either the relationship between the radius of the flame and combustion time or the relationship between pressure and time has to be determined experimentally. In the present investigation, it was decided to obtain the relationship between the radius of the flame and the combustion pressure by using Equation 2.11 derived by Lewis and Von Elbe (13) and the experimentally determined combustion pressure as a function of time. The flame radii calculated in this manner together with the directly measured flame radii are shown in Fig. 4.13. Since the flame front compresses the surrounding acetylene-air mixture adiabatically, the temperature, pressure, and density of the mixture can be found. Using these data, the viscosity coefficient can be found from the air tables under the assumption that the viscosity, of the mixture is the same as that of air. Values of $\frac{\rho_a D}{\mu}$ obtained in this manner, as a function of time, are shown in Fig. 4.15. Now from these values of $\frac{\rho_a D}{\mu}$ the Reynolds number Re as a function of time during combustion was obtained from the relationship shown in Section 2.3. Then the drag coefficient C_D was obtained from Re using the linear-logarithmic approximation given in Table 4.1 and Fig. 4.16. With these values for flame radius R and drag coefficient C_D (the calculations for both have made use of experimentally determined data), the

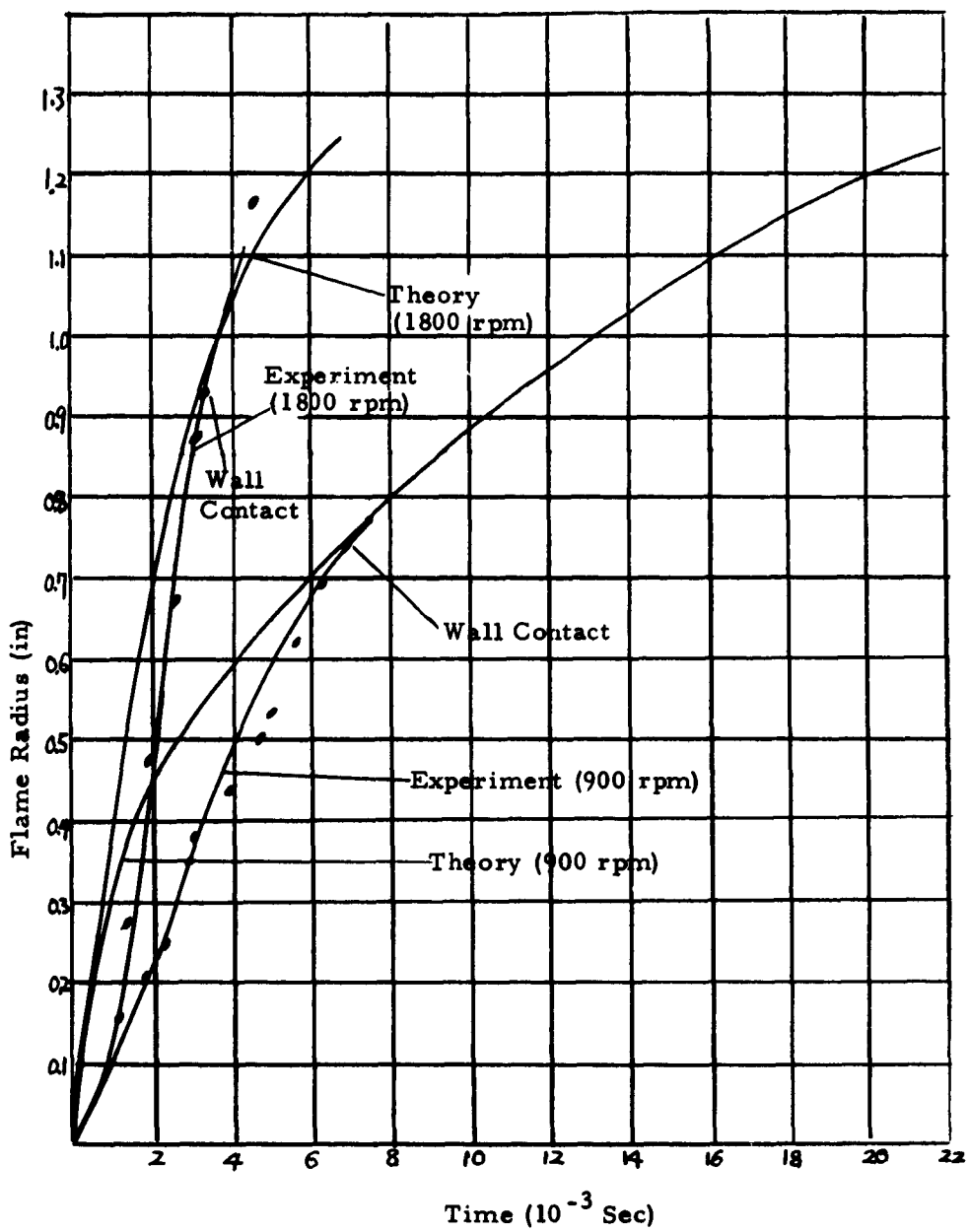

FIG. 4. 13. COMPARISON OF THE FLAME RADIUS DETERMINED BY THE THEORY AND EXPERIMENT.

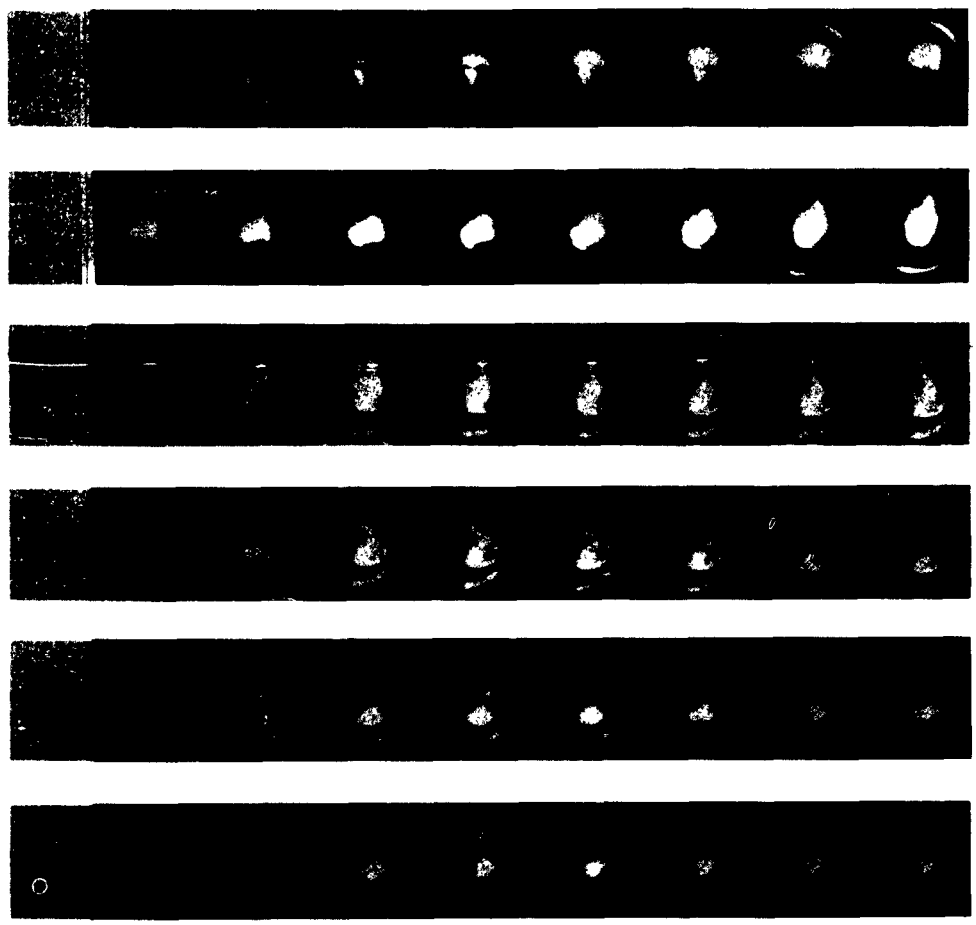

FIG. 4. 14. FLAME PATTERN IN NONHOMOGENEOUS MIXTURE COMBUSTION AT 900 RPM. 3500 FRAMES PER SECOND. 0.3 IN. HG (ACETYLENE) WAS CHARGED TO THE CHAMBER MODEL (PREMIXING TANK: 21 CU. IN.) ANILINE WAS ADDED TO THE PREMIXING TANK. (CONTINUOUS SINGLE FILM STRIP DISPLAYED IN SIX SECTIONS, A THROUGH F.)

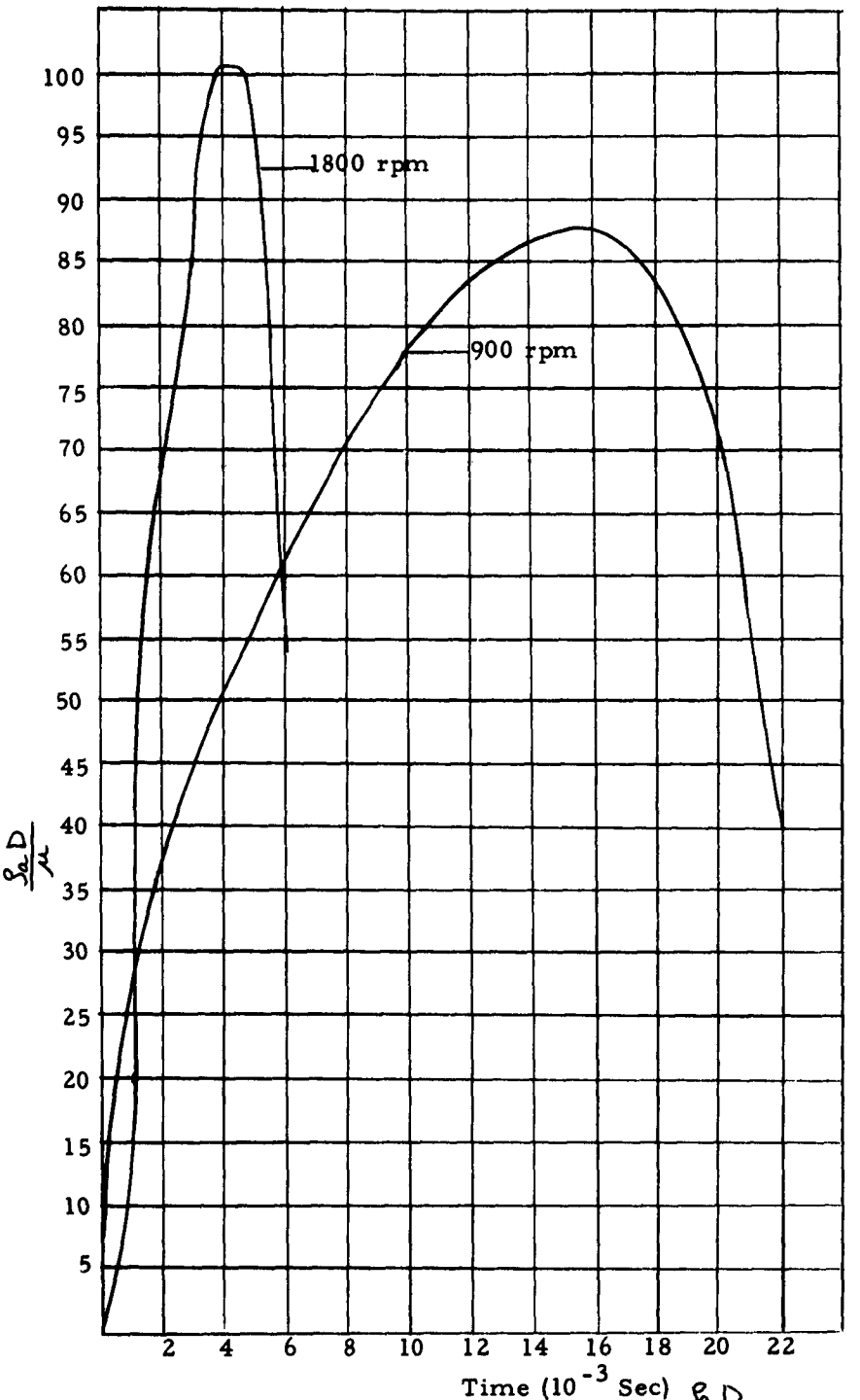

FIG. 4.15. RELATIONSHIP BETWEEN $\frac{\rho a D}{\mu}$ AND COMBUSTION TIME.

TABLE 4.1
APPROXIMATED LINEAR LOGARITHMIC RELATIONSHIP
(Numerical Value)

C_D	Re
0.1 To 1.0	$10\ (Re)^{-0.782}$
1.0 To 10	$10\ (Re)^{-0.552}$
10 To 10^3	$0.557\ (Re)^{-0.239}$
10^3 To 2×10^5	$1.543\ (Re)^{0.0634}$
2×10^5 To 5×10^5	$25.4\ (Re)^{-0.238}$
5×10^5 To 10^6	$0.02\ (Re)^{0.212}$

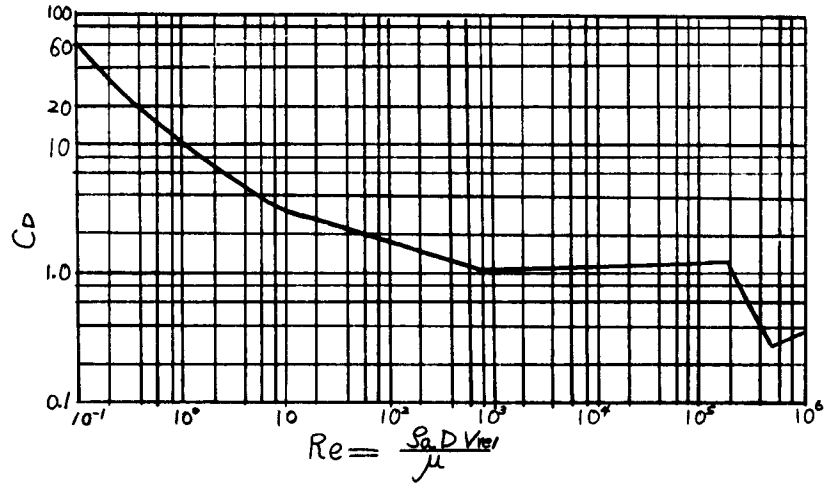

FIG. 4.16. APPROXIMATED LINEAR RELATIONSHIP BETWEEN C_D AND Re.

differential equations for the trajectory of the flame (Equations 2.9 and 2.10) were solved. The calculations were made as described in Appendix II, using an I.B.M. 7074 computer for the theoretical trajectories of the flame for the three cases of the homogeneous mixture ignited at half and three quarter radius from the center and at the periphery under the combustion chamber rotative speeds of 900 and 1800 rpm. The results are shown in Fig. 4.17 (fixed coordinates) and Fig. 4.18 (rotational coordinates). The results of theoretically and experimentally obtained flame trajectories are compared in Fig. 4.11 and Fig. 4.12.

For the purpose of studying the effects of combustion chamber rotative speed and the location of the point of ignition on the magnitudes of the position vector and the tangential velocity of the flame centers, calculations were also made as a function of time for the above mentioned parameters for flame trajectories resulting from ignition effected at half and three-quarter radius from the center and at the periphery under the two different chamber rotative speeds of 900 and 1800 rpm. The results are shown in Fig. 4.17 through Fig. 4.22, for both fixed and rotational coordinate systems. All of these calculations were made under the assumption that the variation of combustion pressure with time was identical in all three cases for the different ignition points at each of the combustion chamber rotative speeds.

The results given in this chapter will be discussed in Chapter V.

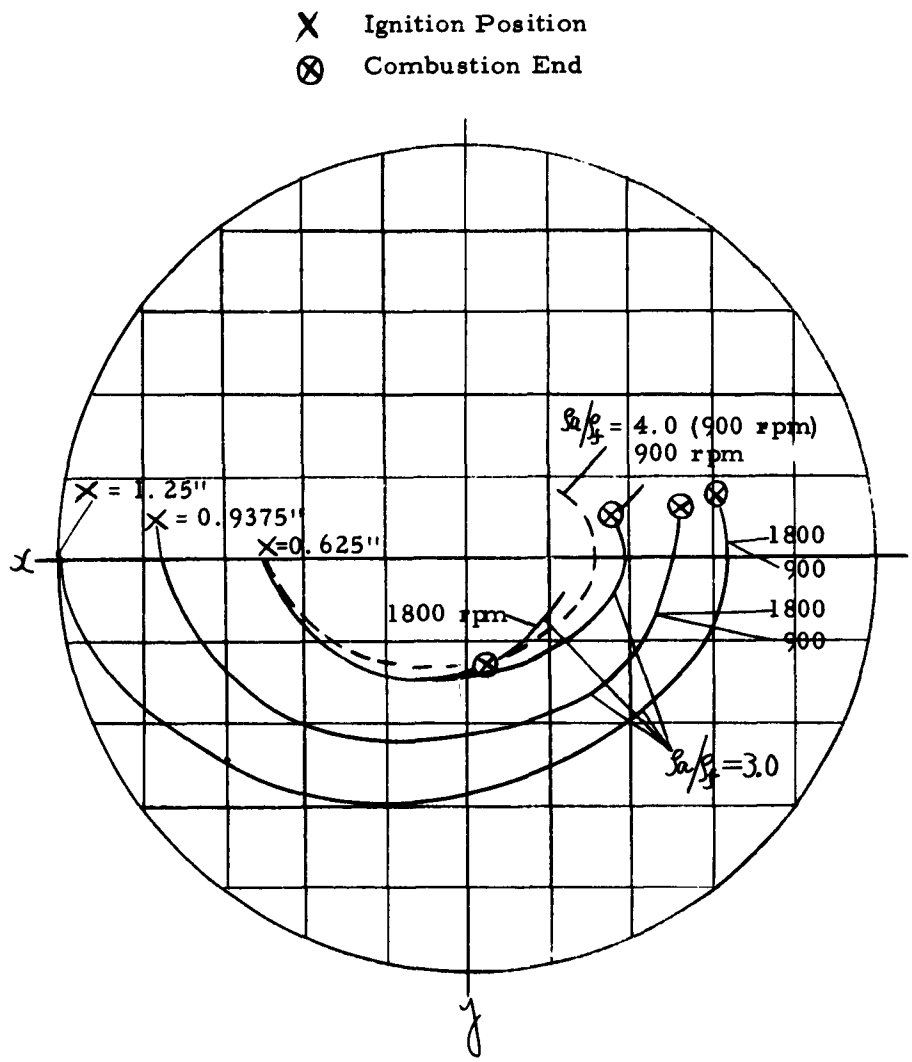

FIG. 4.17. THEORETICAL FLAME TRAJECTORY FOR FIXED COORDINATES.

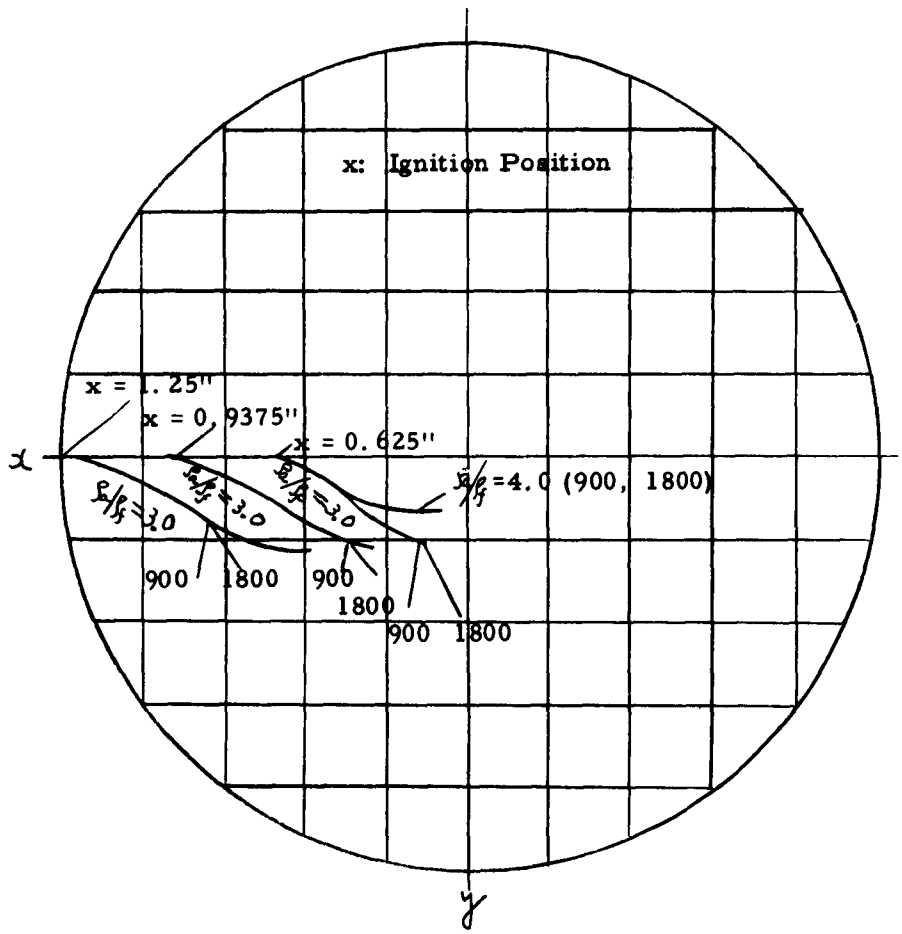

FIG. 4.18. THEORETICAL FLAME TRAJECTORY FOR ROTATIONAL COORDINATES.

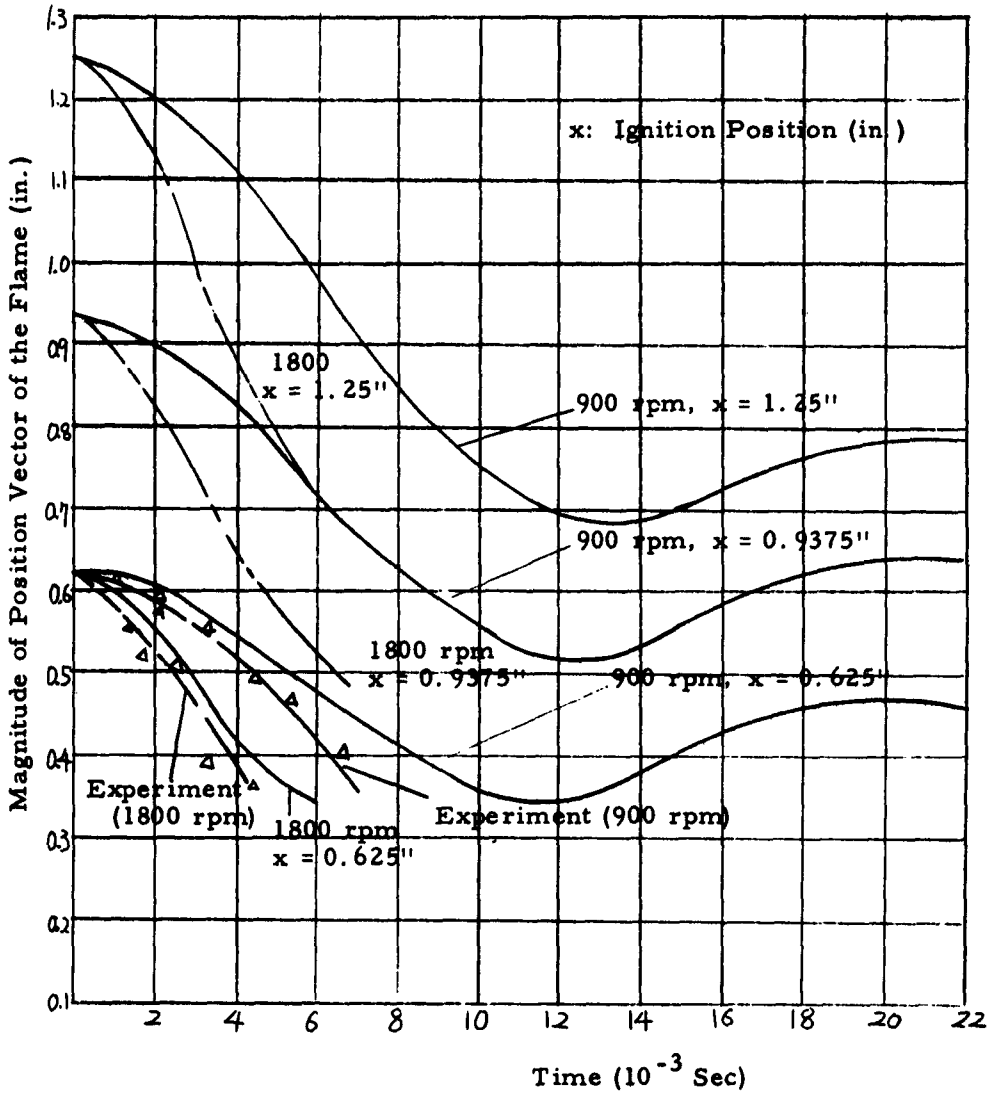

FIG. 4.19. RELATIONSHIP BETWEEN THEORETICAL AND EXPERIMENTAL MAGNITUDE OF POSITION VECTOR OF THE FLAME CENTER AND COMBUSTION TIME FOR FIXED COORDINATES.

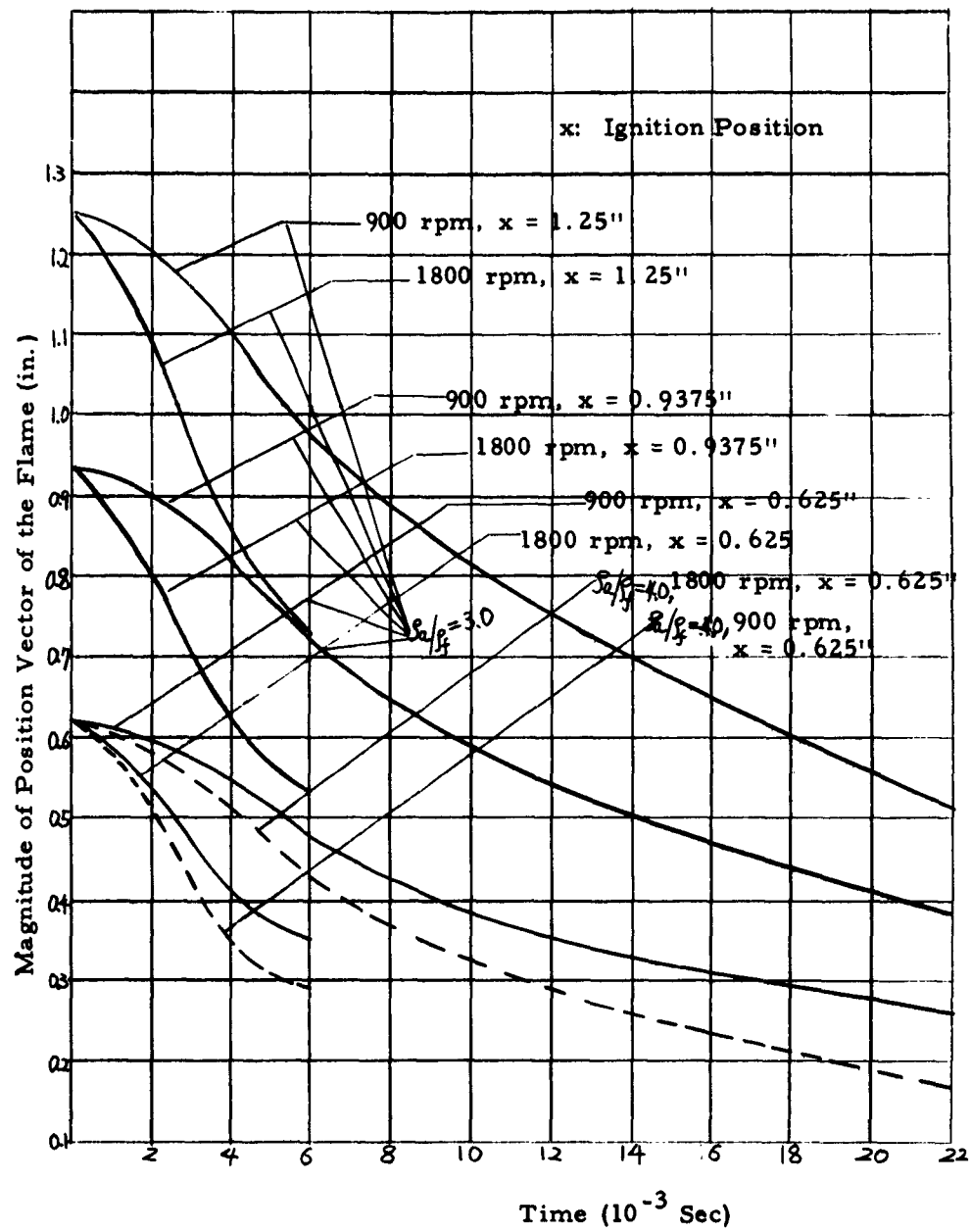

FIG. 4.20. RELATIONSHIP BETWEEN MAGNITUDE OF POSITION VECTOR OF THE FLAME CENTER AND COMBUSTION TIME FOR ROTATIONAL COORDINATES.

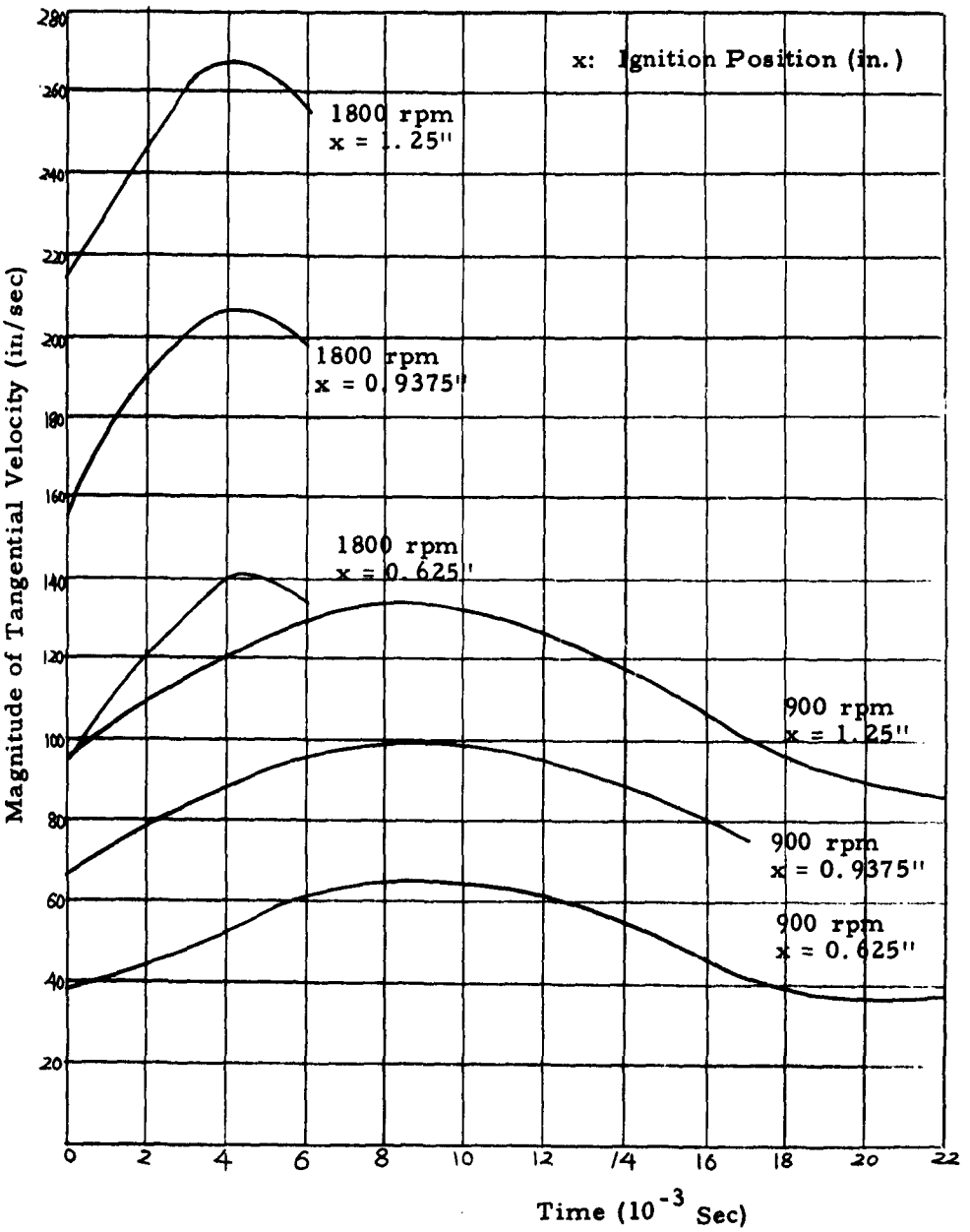

FIG. 4.21. RELATIONSHIP BETWEEN MAGNITUDE OF TANGENTIAL VELOCITY AND COMBUSTION TIME FOR FIXED COORDINATES.

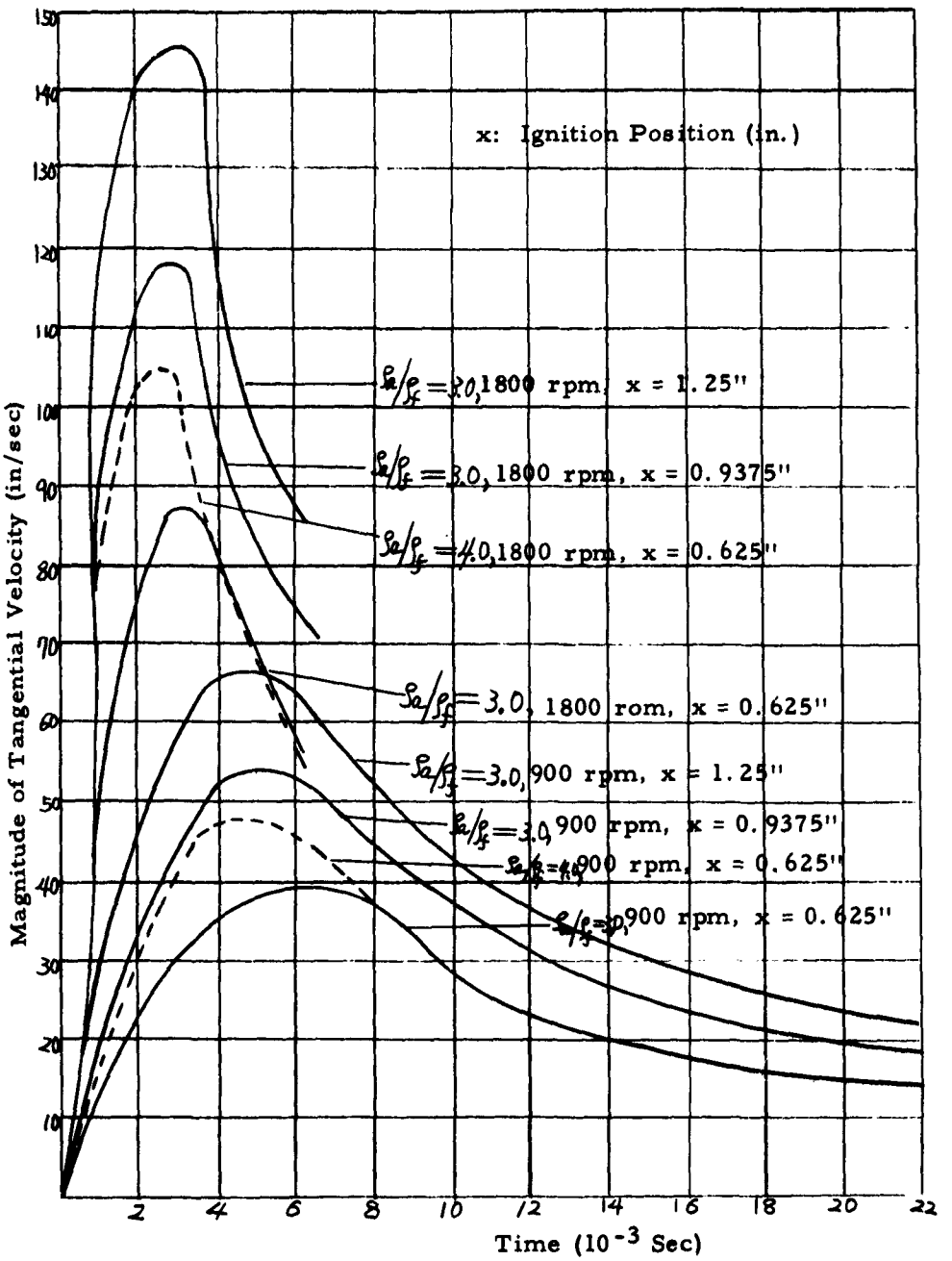

FIG. 4.22. RELATIONSHIP BETWEEN MAGNITUDE OF TANGENTIAL VELOCITY AND COMBUSTION TIME FOR ROTATIONAL COORDINATES.

V. DISCUSSION OF EXPERIMENTAL AND THEORETICAL RESULTS

5.1 Discussion of Experimental Results

When a flame occurs in a swirling field, the flame moves inward to the center of the chamber due to an unbalance of the pressure and drag forces. These forces are considered here to be the only significant forces in the system.

As the flame moves inward during the combustion, the air-fuel mixture will displace outward due to the pressure force, and this motion produces turbulence in the chamber. This turbulence increases the mixing effect between air and fuel even in the case of a mixture which was originally homogeneous before ignition has occurred.

Flame motion changes with the change of rotative chamber speed since the latter results in a change of pressure and drag forces. Furthermore, as the combustion time, flame motion, as related to the combustion time, is dependent upon the chamber rotative speed. Figure 4.1 clearly indicates that the pressure pattern is considerably influenced by rotative chamber speed. These data imply that the combustion time is greatly influenced by the combustion chamber rotative speed, in view of the definition of combustion time given earlier. Throughout these tests, the maximum combustion pressure was found to be nearly constant when the same amount of mixture was charged. That is, the loss of energy is nearly constant during the combustion at different speeds.

As shown in Fig. 4. 5, when ignition takes place at the periphery, the combustion time is influenced by the chamber rotative speeds. The pressure force acting on the flame in the case of high speeds is larger than that of the case of stationary and low chamber rotative speeds; thus, showing that the pressure force has a definite effect on combustion time. At comparatively high speeds, the change in combustion time becomes small since the flame front moves very rapidly due to the greater pressure force, without experiencing perfect combustion. The gas which could not burn perfectly is converted to smoke behind the flame front and therefore the change in combustion time with respect to combustion chamber rotative speed becomes small at high speeds. The difference between the combustion time for peripheral, half radius, and center ignition as indicated in Fig. 4. 5, is mainly due to the differences in the area of the burning surface and in the wall effect. This is true both in the case of homogeneous and nonhomogeneous mixture combustion. In the case of peripheral ignition, the flame configuration is not cylindrical and the burning surface area is smaller than in the cases of half radius from the center or center ignitions. The time variation of the pressure, which was recorded with the Polaroid camera, is not much different until the wall effect becomes important, as shown in Fig. 5. 1. The graph was obtained for methane-air mixture charged into the stationary chamber in the case of Part (c). In the case of center ignition (refer to the description in 3. 1. 1), the chamber rotative speed does not influence the combustion time because the pressure

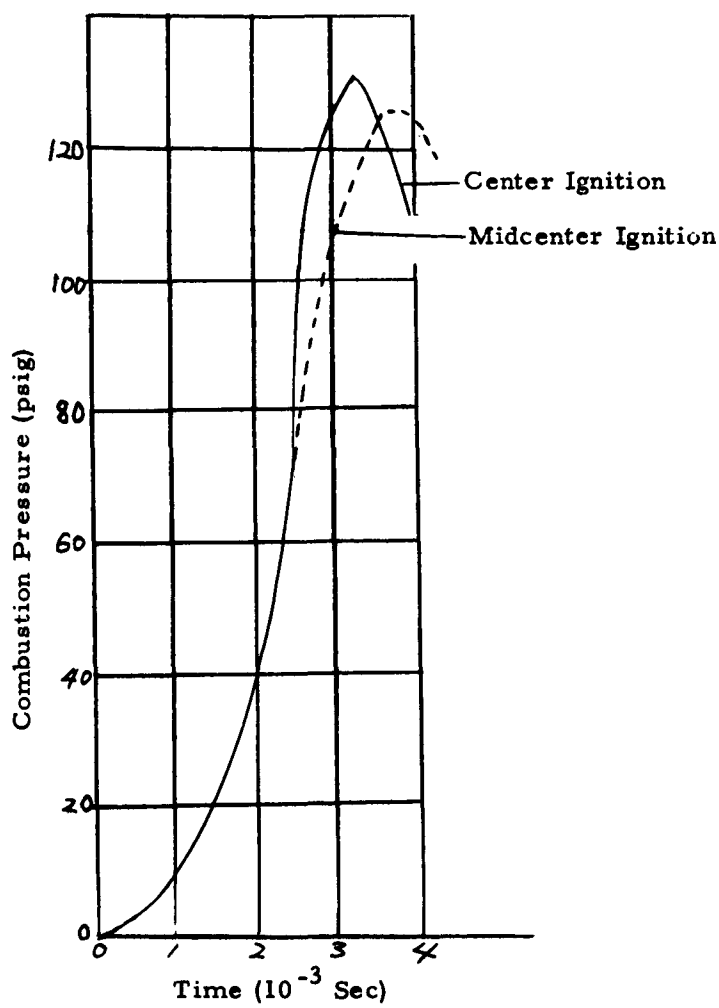

FIG. 5.1. COMPARISON OF COMBUSTION PRESSURE VS. COMBUSTION TIME WHEN IT WAS IGNITED AT HALF RADIUS FROM CENTER AND CENTER.

is zero at the geometric center. Therefore a trajectory does not exist in this case, and the flame will propagate radially. This is equivalent to the case of the fundamental Equation 2.9 with all the boundary conditions equal to zero, which makes the case trivial.

As shown in Fig. 4.6, as the chamber rotative speed is increased, the combustion time decreases for each of the three ignition positions with nonhomogeneous mixture combustion and with the mixture charged at the periphery. The reason is that during combustion, the nonhomogeneous, overrich mixture at high chamber speeds becomes a comparatively lean mixture in the central area of the chamber due to forced diffusion. It is believed that such a lean mixture resulting at high speeds is more suitable for combustion than the richer mixture present at low speeds. The speed of the chamber has a great effect on the combustion time in the case of center ignition; for, as the rich mixture was charged at the periphery, diffusion occurred due to the pressure gradient which has a direct relationship to the chamber speed. The mixture at the geometrical center becomes lean compared with the mixture around the charging port. This condition is believed to be more suitable for combustion; that is, the flame which originates at the geometrical center will propagage itself radially with a high speed at the prevailing lean mixture ratio.

When the fuel was charged at half radius from the center, the effect of combustion chamber rotative speed on combustion

time was exactly opposite from that for the results shown in Fig. 4.6, obtained when charging was effected at the periphery. As shown in Fig. 4.7, combustion time increases with an increase in chamber speed. The reason for this is that part of the rich mixture diffuses toward the geometrical center, due to the pressure gradient, while another portion of the rich mixture will diffuse toward the wall due to the temperature gradient caused by the heat of friction between the journal bearing and hollow cylinder produced by the chamber rotation. But the main portion of diffusion is believed to be the forced diffusion due to the pressure gradient rather than the thermal diffusion. When the point of ignition was located at the periphery of the chamber, the flame around the periphery propagated more rapidly than that around the charging port; and as the flame front arrived near the center where acetylene was concentrated due to force diffusion from the charging port, flame speed decreased further from that around the periphery. Finally, the flame passed through the center and propagated toward the lean mixture zone formed near the wall opposite to the ignition point. Thus the most unsuitable region for combustion was considered to be around the center in the case of charging at half radius from the center. In other words, the concentration of the acetylene-air mixture around the center increased with the increase in chamber speed and caused the flame speed to decrease around the center.

Therefore combustion time increased with the increase of rotative chamber speed. For a given value of rotative chamber speed, the combustion time was found to be the shortest for the center ignition and the largest for the peripheral ignition. This fact may be due to the larger burning surface area that occurs with center ignition and the smaller burning surface area that occurs with peripheral ignition.

As shown in Fig. 4.8, in the case of homogeneous mixture combustion of a rich mixture, the chamber rotative speed has more effect on combustion time than that in the case of a non-homogeneous mixture combustion. This condition is due to the fact that, in the case of homogeneous mixture combustion, the higher the combustion chamber rotative speed the higher the pressure gradient becomes, and in turn, the higher the speed of flame propagation becomes.

In the case of nonhomogeneous mixture combustion the mixture ratio varies throughout the chamber due to the pressure gradient and the temperature gradient. The distribution of the mixture ratio in the nonhomogeneous case is better for combustion than that of the homogeneous mixture. Based on the above given argument, it can be said that the relationship between combustion time and chamber rotative speed is less pronounced in the case of nonhomogeneous mixture combustion than in the case of homogeneous mixture combustion.

As a counterpart of the experiments carried out with an overrich mixture Part (e) and (g), a similar experiment was carried out with a lean acetylene-air mixture with a ratio of 1:6.4 (acetylene of 10 inches of mercury above atmospheric pressure and air of 28 inches of mercury above atmospheric pressure) charged into the combustion chamber (0.3×10^{-4} lb). Combustion time was found to be shorter for the homogeneous mixture combustion than for the nonhomogeneous mixture combustion. In the case of nonhomogeneous mixture combustion, combustion time increased with increasing chamber speed; whereas, in the homogeneous mixture combustion, combustion time decreased with an increase in the rotative chamber speed. The reason can be explained as follows. A mixture ratio of 1:64 is close to a stoichiometric ratio; and, in the case of homogeneous mixture combustion, combustion time decreased with an increase in chamber rotative speed due to the pressure force. However, in the case of nonhomogeneous mixture combustion, the mixture ratio became leaner toward the center due to forced diffusion; and near the center, the mixture ratio decreased to the extent that the speed of flame propagation is reduced greatly (14).

The above explanation leads to the conclusion that nonhomogeneous mixture combustion, such as that in a high speed diesel engine, can provide larger values of time rate of energy emission than the homogeneous mixture combustion, provided an overrich mixture is used at high swirl rates.

In the experiment with nonhomogeneous mixture combustion, a pressure spike was observed during the combustion process. In order to determine the origin of this spike, a one dimensional cylindrical chamber (with a length much greater than the diameter), shown in Fig. 5.2, was constructed. First a pressure pickup with a connecting tube was attached, and then a pressure pckup without a connecting tube was attached to this combustion chamber in an effort to determine the cause of the pressure spike. The experiment was carried out for the nonhomogeneous case using both rich and lean mixtures. The rich and lean acetylene-to-air mixture ratio (by weight) was 1:4.85 and 1:6.4 respectively. Fuel and air were mixed in the premixing tank and charged into the combustion chamber until the pressure in the premixing tank decreased to 2 inches of mercury equivalent to an outflow of 0.605×10^{-4} lb. The relationship between combustion pressure and time was recorded using the Polaroid camera.

The results are shown in Fig. 5.3 (a) and (b), where it is noted that a pressure spike was observed only during the tests with the pressure pickup which had a connecting tube. The results of these tests indicate the following to be the cause of the pressure spike. The small tube which is connected to the pressure pickup will be filled with combustible gas when an overrich mixture is charged into the chamber and it will burn out as the flame front passes the geometrical center of the chamber. The burning gas will cause the pressure in the

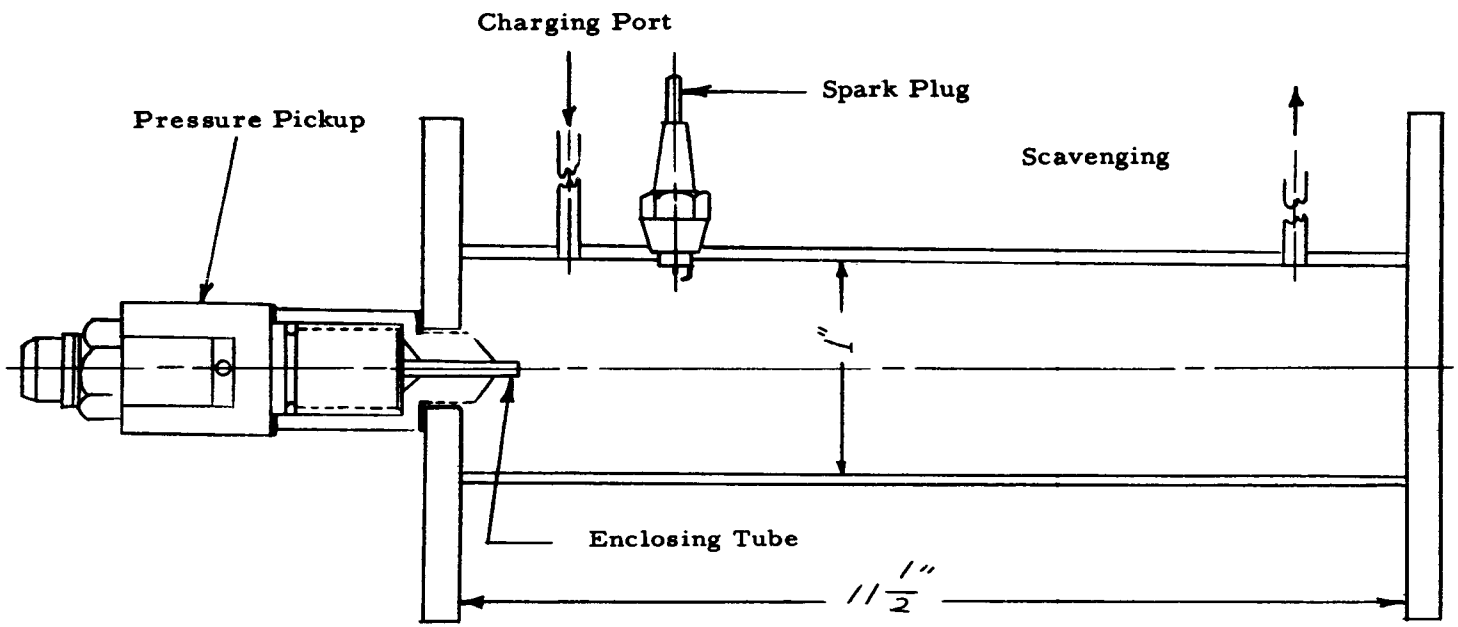

FIG. 5.2. ONE DIMENSIONAL COMBUSTION CHAMBER MODEL FOR THE PRESSURE SPIKE.

a) RELATIONSHIP BETWEEN PRESSURE AND COMBUSTION TIME AT A RICH MIXTURE WHEN THE PRESSURE PICKUP, WITHOUT THE TUBE, WAS USED IN A ONE-DIMENSIONAL CHAMBER.

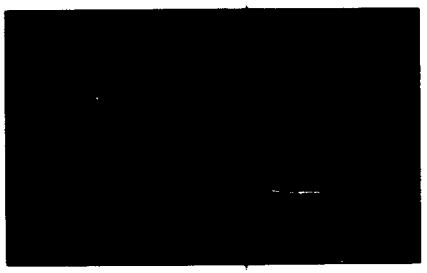

b) RELATIONSHIP BETWEEN PRESSURE AND COMBUSTION TIME AT RICH MIXTURE WHEN THE PRESSURE PICKUP WITH THE TUBE, WAS USED IN ONE-DIMENSIONAL CHAMBER.

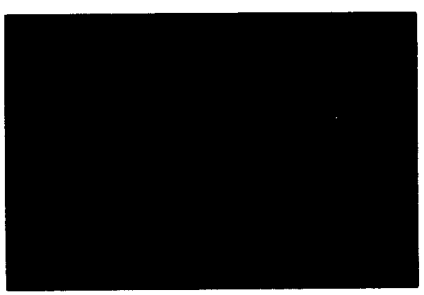

c) RELATIONSHIP BETWEEN PRESSURE AND COMBUSTION TIME IN A HOMOGENEOUS MIXTURE. COMBUSTION OCCURRED AT 500 RPM BY PERIPHERY IGNITION (PRESSURE PICKUP WITHOUT THE TUBE).

d) RELATIONSHIP BETWEEN PRESSURE AND COMBUSTION TIME IN A NONHOMOGENEOUS MIXTURE. COMBUSTION OCCURRED AT 1350 RPM BY PERIPHERY IGNITION (PRESSURE PICKUP WITH THE TUBE).

FIG. 5. 3. PHOTOGRAPHIC RECORD OF PRESSURE SPIKE PHENOMENA.

tube to rise very rapidly because the volume of the tube is small. The burning gas, with rising pressure, will produce a jet into the main combustion chamber due to the pressure difference between the tube and the main combustion chamber and cause the pressure to decrease very rapidly in the tube. Thus it can be concluded that the occurence of the pressure spike is due to a phenomenon that has no effect on the combustion time in cases as (d) of Fig. 5.3. The pressure spike did not appear with either of the pressure pickup installation in lean mixture combustion because the mixture in the tube did not burn.

5.2 Discussion of Photographic Results

As shown in Fig. 4.2 and Fig. 4.3 for the homogeneous case, a strong swirl was observed as the flame disappeared. This swirl is considered to be caused by the inward movement of the flame during the early stages of the combustion. When the acetylene-air mixture as specified in Part (h) of Table 3.1 was charged into the combustion chamber at the half radius from the center and ignited at half radius at 900 rpm, the flame was observed to spiral around the geometrical center in the later stage of combustion. The experimental methods are not idealized enough to permit comparison with the theoretical results which were obtained under the assumption that the flame is circular.

In finding the flame trajectory experimentally, it is advantageous to study the nonhomogeneous mixture combustion in which the flame can propagate symmetrically about the flame

center. In the nonhomogeneous case, the rich mixture slug charged into the chamber will remain circular in the ideal case, and one can expect to have a flame which expands adiabatically and symmetrically about the flame center in the mixture. Then, as the flame expands, the boundary of the acetylene-air mixture will be displaced outward by the flame front. The flame center will deviate from the initial center due to the pressure force. At the last stage of combustion, the flame front will coincide with the boundary of the expanding mixture. In the diesel case, the form of the flame is circular; and this flame will move for a while until it diminishes. Consequently, one can observe the flame trajectory by photographing the flame with a high speed camera. In this case, if the maximum radius of the flame is small compared to the radius of the combustion chamber, the drag force will be proportional to the square of the relative velocity of the flame. Thus the original differential equation will apply, even for the later portion of the combustion. This condition may be true ideally; however, in the experimental work it was found that, for the nonhomogeneous case, the flame was not quite circular, as shown in Fig. 4. 14. This caused the measured results to differ from the theoretical predictions. Therefore, the measurements for the homogeneous case, ignited at the point half radius from the center, shown in Fig. 4. 9 and Fig. 4. 10, were used for comparison with the theoretical predictions. It can be seen that in the early stage of the combustion the flame follows the original assumption that the flame

is circular until the wall effect becomes appreciable.

5.3 Discussion of Theoretical Results

As shown in the Fig. 4.16 and Fig. 4.17, the trajectory of the flame in the case of high chamber rotative speeds is almost the same as that of the case of lower speeds. If the drag force is neglected and the pressure force is considered as the only force acting on the system, the trajectory of the flame has no relation to the chamber speed as shown by Equation 2.15. Conversely, if we neglect the pressure force and consider the drag force as the only force acting on the flame, the flame trajectory (solution of Equation 2.16) is found to be almost independent of the combustion chamber rotative speed. Therefore, we can postulate that the actual flame trajectory is almost independent of the chamber rotative speed. However, the rate of change of the radius of curvature of the flame trajectory in the case of 1800 rpm is almost twice that of the case of 900 rpm. (Refer to Fig. 4.19 and Fig. 4.20)

If we consider that both the pressure and drag forces are acting on the flame, the trajectory of the flame will deviate from an elliptical curve toward the inside due to the drag force as shown in Fig. 5.4 (solution of Equation 2.9). The deviation of the trajectory from an elliptical path is very slight at the beginning of combustion since the drag force acting on the flame is very small because the tangential velocity is almost the same as the rotative chamber speed at the beginning of combustion, as shown in Fig. 5.4 and Fig. 5.5.

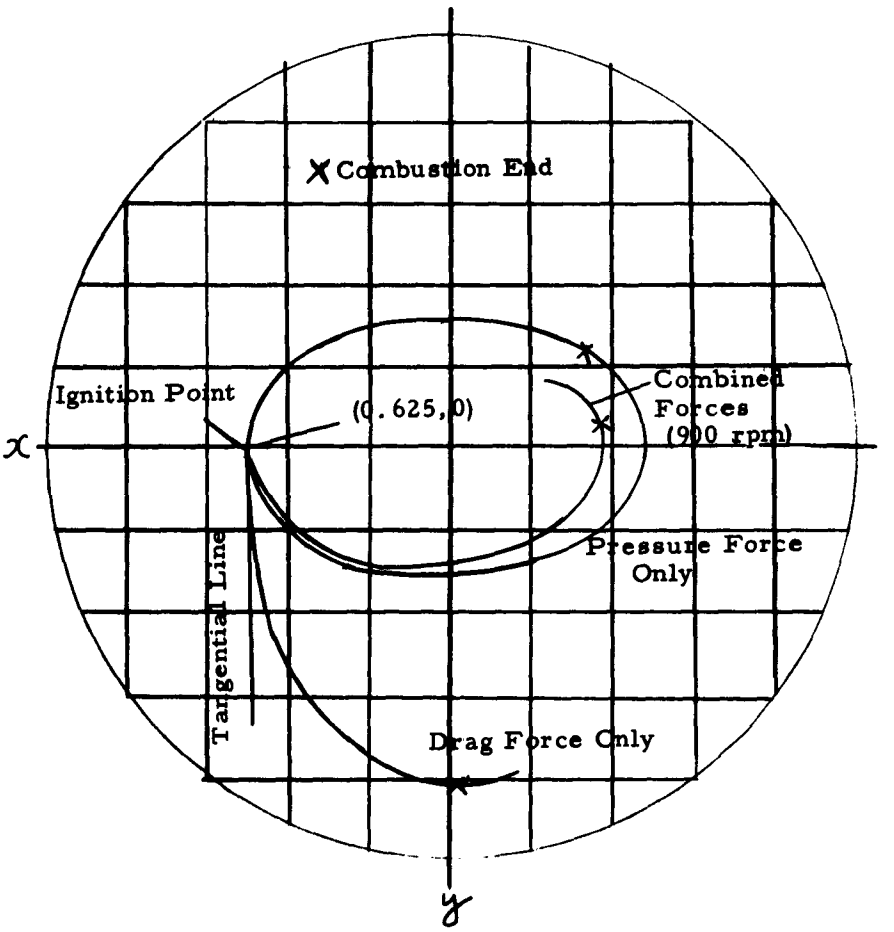

FIG. 5.4. COMPARISON OF FLAME TRAJECTORY IN CASE OF ONLY PRESSURE FORCE ACTING OR ONLY DRAG FORCE ACTING AS THE FICTITIOUS CASE AND COMBINED FORCES ACTING ON THE FLAME FOR FIXED COORDINATE SYSTEM.

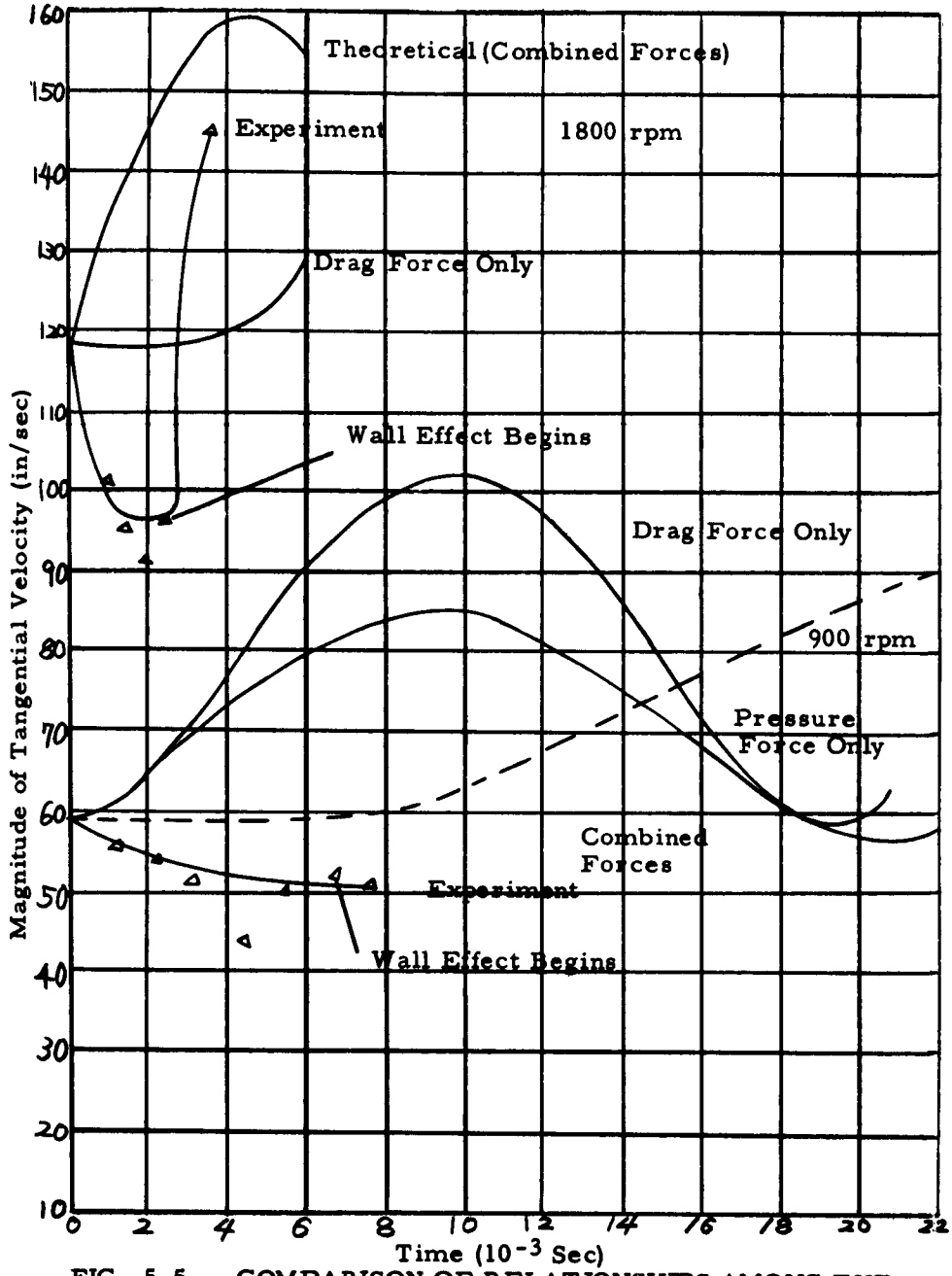

FIG. 5.5. COMPARISON OF RELATIONSHIPS AMONG THE MAGNITUDE OF TANGENTIAL VELOCITY VS. COMBUSTION TIME IN CASE OF ONLY PRESSURE FORCE ACTING OR ONLY DRAG FORCE ACTING AND COMBINED FORCES ACTING ON THE FLAME.

The radius of curvature of the flame trajectory becomes smaller as the mixture-to-flame density ratio increases, as shown in Fig. 4. 17 and Fig. 4. 18. This change is due to the unbalanced forces. This conclusion was reached under the assumption that the combustion time and pressure are the same as that in the case of ignition at the point half a radius from the center. As shown in Fig. 4. 20, the magnitude of the position vector of the flame is smaller in the case where $\frac{\rho_a}{\rho_f} = 4.0$ than that of the case where $\frac{\rho_a}{\rho_f} = 3.0$.

The tangential velocity of the flame for the combustion chamber rotative speed of 1800 rpm is almost twice that of the case when the chamber rotative speed was 900 rpm, as shown in Fig. 4. 21 and Fig. 4. 22. This means that the drag force, which affects the mixing process, will increase by a factor of about four because the drag force is proportional to the square of relative velocity. Furthermore, the results shown in Fig. 4. 21 and Fig. 4. 22 imply that stronger mixing of the fuel-air mixture is produced if ignition is effected at a larger radial distance from the center. This conditions is so because fuel-air mixing depends upon the tangential velocity of the flame which is affected by the position of the point of ignition.

The tangential velocity increases as the mixture to flame density increases as shown in Fig. 4. 22.

If we neglect the drag force and consider the hypothetical case where the pressure force is the only force acting on the flame, then the absolute value of the position vector of the flame

center is periodic and will have a minimum value at (0, $0.625/\sqrt{3}$) as shown in Fig. 5.4. In the practical case--that is, when both pressure and drag forces are acting--the magnitude of the position vector has a minimum value that is smaller than that of the above-mentioned hypothetical case because of the drag force. The drag force corresponds to a damping force in a mass-spring system.

As observed in Equation 2.15, when the mixture-to-flame density ratio increases, the flame center describes a slender ellipse. For example, when ignition occurs at (0.625, 0) with $\frac{\rho_a}{\rho_f} = 4.0$, the major and minor axes of the ellipse are 0.625 and 0.625/2 respectively. In the ultimate case, if the density ratio ($\frac{\rho_a}{\rho_f}$) becomes infinite, the flame motion becomes a simple harmonic motion. Therefore, one can predict that a flame occurring in a mixture which has larger value of ρ_a/ρ_f will move inside of the trajectory of a flame occurring in a mixture having a smaller value of ρ_a/ρ_f.

As shown in Fig. 4.22, the magnitude of the tangential velocity of the flame, in a rotational coordinate system, and in the case of $\frac{\rho_a}{\rho_f} = 4.0$, is larger than that of the case of $\frac{\rho_a}{\rho_f} = 3.0$. Therefore, in the practical case, it can be predicted that combustion, where $\frac{\rho_a}{\rho_f} = 4.0$, is better than that where $\frac{\rho_a}{\rho_f} = 3.0$ because the greater drag force acts in the former case, and the greater drag force causes better mixing and therefore better combustion.

According to Fig. 5.4, the flame trajectory resulting from

the pressure force alone almost coincides with the flame trajectory obtained when the combined forces are considered; whereas, the trajectory resulting from the drag force alone deviates considerably from that of the combined forces. This leads to the conclusion that the flame trajectory is determined predominantly by the pressure force.

As a hypothetical case, if one considers that the pressure force is the only force acting on the flame, the relationship between the tangential velocity of the flame and time is a periodic function of time, and the flame motion follows Kepler's second principle, as shown in Fig. 5. 5.

In the case where the drag force is considered as the only force acting on the flame, the tangential velocity is $0.625\,\omega$ which is comparable to the combustion chamber rotative speed at the beginning of combustion; that is, at the beginning the drag force is almost negligible, as shown in Fig. 5. 5. As the drag force increases with time, the flame deviates from the tangential line at (0. 625, 0), and the rate of deviation from the tangential line in Fig. 5. 4 will cause the actual flame trajectory to describe a spiral curve inside of the elliptical trajectory which was obtained from the hypothetical case.

As shown in Fig. 5. 5, the magnitude of the tangential velocity of the flame will increase to a maximum which is caused by the pressure force. As the drag force increases, this increase will decelerate the magnitude of the tangential velocity of the flame.

5.4 The Comparison of the Experimental and Theoretical Results for the Flame Trajectory.

Figure 4.17 and Fig. 4.18 show the flame trajectory which was obtained by theoretical calculations for fixed and rotational coordinates. Figure 4.11 and Fig. 4.12 show the comparison of the theoretical and experimental trajectories of the flame. At the beginning of combustion, both curves coincide; but, in the later portion of the combustion, the curves deviate considerably due to the wall effect and the drag force. In the calcaulation of the drag force, it was assumed that the boundary line of the flame is distinct; but, in the practical case the boundary line is not distinct; and, when the flame grows to a large size compared with the size of the chamber, the drag force is no longer proportional to the square of the relative velocity. The expanding flame does not follow the adiabatic process, see Fig. 4.14. As shown in Fig. 5.5, the experimental magnitude of the tangential flame velocity is smaller than that of the theoretical calculation; also, as shown in Fig. 4.20, the magnitude of the measured position vector of the flame is smaller than that of the theoretical calculation because the drag force acting in the practical case is larger than that assumed in the theoretical case, even in the early stages of the combustion.

5.4 The Comparison of the Experimental and Theoretical Results for the Flame Trajectory.

Figure 4.17 and Fig.4.18 show the flame trajectory which was obtained by theoretical calculations for fixed and rotational coordinates. Figure 4.11 and Fig.4.12 show the comparison of the theoretical and experimental trajectories of the flame. At the beginning of combustion, both curves coincide; but, in the later portion of the combustion, the curves deviate considerably due to the wall effect and the drag force. In the calcaulation of the drag force, it was assumed that the boundary line of the flame is distinct; but, in the practical case the boundary line is not distinct; and, when the flame grows to a large size compared with the size of the chamber, the drag force is no longer proportional to the square of the relative velocity. The expanding flame does not follow the adiabatic process, see Fig.4.14. As shown in Fig.5.5, the experimental magnitude of the tangential flame velocity is smaller than that of the theoretical calculation; also, as shown in Fig.4.20, the magnitude of the measured position vector of the flame is smaller than that of the theoretical calculation because the drag force acting in the practical case is larger than that assumed in the theoretical case, even in the early stages of the combustion.

VI. SUMMARY AND CONCLUSION

6.1 Statement of the Problem

The purpose of this investigation was to investigate the trajectory of the flame in a swirling field by theoretical and experimental methods. In addition, the effect of the rotative combustion chamber speed on the combustion time in homogeneous and nonhomogeneous mixture combustions was investigated.

The results of the theoretical work were compared with the experimental results in finding the trajectory of the flame in the swirling field of the combustion chamber.

6.2 Procedure and Results

The first part of this work was the investigation of the effects of the rotative combustion chamber speed on the combustion time in homogeneous and nonhomogeneous mixtures using both methane and acetylene gas.

The second part of this work was the investigation of the trajectory of the flame in homogeneous mixtures using acetylene gas as fuel. A high speed camera was used to record the visual observations.

Test results show that the combustion chamber rotative speed has an influence on the combustion time. It has been found that the optimum location of the point of ignition is at the periphery in both homogeneous and nonhomogeneous mixture combustion. In the homogeneous mixture combustion, the effects of combustion

chamber rotative speed on the combustion time was greater than that of the nonhomogeneous mixture combustion for rich mixtures, but the condition of combustion in the nonhomogeneous case was better than that of the homogeneous mixture combustion. For lean mixtures, the homogeneous mixture has better combustion conditions than that of the nonhomogeneous mixture combustion.

The theoretical trajectory of the flame almost coincides with the experimentally determined trajectory of the flame at the beginning portion of the combustion. If the density ratio of the air to the flame increases, one can predict that the combustion time will decrease and thermal mixing will improve.

Comparing the magnitude of the tangential velocity of the theoretical and experimental results, it was found that the drag force, in the experimental case, was larger than that of the theoretical calculation.

The larger deviation between the theoretical and experimental flame trajectories at the later portion of the combustion may be caused by the inaccurate calculation of the drag force and the wall effect.

6.3 Conclusions

The optimum ignition position is on the periphery of the chamber because the flame can then introduce the strongest swirl in the chamber for both the case of homogeneous and of nonhomogeneous mixture combustion.

It can be expected that the nonhomogeneous case will provide better burning conditions than that of the homogeneous mixture combustion. The swirling effect in the homogeneous mixture combustion, however, is better than that of the nonhomogeneous mixture combustion for rich mixtures.

At the beginning of the combustion, the experimentally observed trajectory of the flame coincides with the theoretical trajectory; thus the original assumptions can apply to the practical problem during the early period of the combustion. But in the later portion of the combustion, the assumptions for the drag force made in this study must be modified.

6.4 Suggestions for Further Work

It is very important to investigate the flame trajectories as they occur in actual engines as a means of improving combustion. Some theoretical analogy should be found that will more nearly approximate the conditions found in actual engines. When the flame grows to a larger size, the drag force is no longer proportional to the square of the relative velocity. Thus, a number of areas exist wherein a more precise analysis is needed in order to obtain a better determination of the drag force.

BIBLIOGRAPHY

1. A. and F. Pischinger, Der Einflus der Wand bei der Verbrennung eines Brennstoffstrahles in einem Luft Wirbel, M.T.Z., Vol. 20, No. 1, 1959, p. 4.

2. F. Nagao and H. Kakimoto, Kraftstoffeinspritzung und Verbrennung in der Wirbelkammer des Dieselmotors, M.T.Z., Vol. 20, No. 6, 1959, p. 183.

3. J. S. Meurer, Multifuel Engine Practice, S.A.E. Transactions, Vol. 70, p. 712, 1962.

4. F. Eisfeld, Der Einfluss die Luftbewegung auf die Kraftstoffverteilung im Brennraum eines Dieselmotors mit Luftdrehung, Doctorial Thesis, 1960, Technische Hochschule Braunschweig, Germany.

5. A. R. Kriebel, Particle Trajectory in a Gas Centrifuge, Transaction of ASME, Journal of Basic Engineering, Vol. 83, September 1961, p. 333.

6. K. L. Calder, Some Theoretical Aspects of the Rotating Drum Aerosol Chamber, BWL Technical Study No. 13, October 1958, Army Biological Warfare Laboratory, Fredrick, Md. (ASTIA: AD 207 865).

7. A. W. Hussmann, F. Kahoun and R. A. Taylor, Studies of Stratification by Fuel Injection into Swirling Air, S.A.E. Preprint 598A of the 1962 National Powerplant Meeting, November 1962.

8. S. D. Raezer, The Relation Between Burning Velocity and Space Velocity of a Spherical Combustion Wave in a Closed Spherical Chamber, Combustion & Flame, Vol. 5, No. 1, 1961, p. 77.

9. A. S. Campell, The Time Required for the Constant Volume Combustion, ASME Trans., Vol. 74, 1952, p. 72.

10. F. Nagao, T. Kobayagawa and F. Adachi, Stationary Flame Front in a Swirl Combustion chamber, Bulletin of J.S.M.E., Vol. 1, No. 2, 1958, p. 151.

11. D. G. Udelson, Geometrical Considerations in the Burning Liquid Drops, Combustion & Flame, Vol. 6, No. 2, June 1962, p. 93.

BIBLIOGRAPHY, Continued

12. H. Kakimoto, Swirl and Combustion in Divided Combustion Chamber Type Diesel Engines, Ph. D. Thesis, Dept. of Mechanical Engineering, University of Kyoto, Japan, 1960, p. 5.

13. B. Lewis and G. Von Elbe, Combustion, Flames and Explosion, Academic Press Inc., New York, N. Y., 1951.

14. W. A. Bone and D. T. A. Townend, Flame and Combustion in Gases, Longmans, Green and Co., Ltd, New York, N. Y., 1927, p. 114.

15. K. S. Kunz, Numerical Analysis, McGraw-Hill, New York, N. Y., 1957.

APPENDIX I
MATHEMATICAL DERIVATION

Numerical Solution of The Flame Trajectory Equations

From Chapter II, Equation 2.5, the original equation of the flame trajectory for fixed coordinates is:

$$\ddot{\bar{z}} = -\frac{3C_D}{\pi R}\left|\dot{\bar{z}} - i\bar{z}\omega\right|\left(\dot{\bar{z}} - i\bar{z}\omega\right) - 3\bar{z}\omega^2 \qquad A.1$$

Dividing this into its real and imaginary parts results in:

$$\ddot{x} + i\ddot{y} = -\frac{3C_D}{\pi R}\sqrt{(\dot{x}+y\omega)^2+(\dot{y}-x\omega)^2}\left[(\dot{x}+y\omega)+i(\dot{y}-x\omega)\right] - 3(x+iy)\omega^2$$

where

$$\left.\begin{aligned}\ddot{x} &= -\frac{3C_D}{\pi R}\sqrt{(\dot{x}+y\omega)^2+(\dot{y}-x\omega)^2}\,(\dot{x}+y\omega) - 3x\omega^2\\ \ddot{y} &= -\frac{3C_D}{\pi R}\sqrt{(\dot{x}+y\omega)^2+(\dot{y}-x\omega)^2}\,(\dot{y}-x\omega) - 3y\omega^2\end{aligned}\right\} \qquad A.2$$

Applying the same procedure to Equation 2.8 Chapter II, for the rotational coordinate system results in:

$$\left.\begin{aligned}\ddot{\xi} &= -\frac{3C_D}{\pi R}\left(\dot{\xi}^2+\dot{\zeta}^2\right)^{\frac{1}{2}}\dot{\xi} + 2\omega\dot{\zeta} - 2\omega^2\xi\\ \ddot{\zeta} &= -\frac{3C_D}{\pi R}\left(\dot{\xi}^2+\dot{\zeta}^2\right)^{\frac{1}{2}}\dot{\zeta} - 2\omega\dot{\xi} - 2\omega^2\zeta\end{aligned}\right\} \qquad A.3$$

The generalized form of Equations A.2 and A.3 is as follows:

$$\left.\begin{aligned}\ddot{x} &= f(\dot{x},\dot{y},x,y)\\ \ddot{y} &= g(\dot{x},\dot{y},x,y)\\ \ddot{\xi} &= F(\dot{\xi},\dot{\zeta},\zeta,\xi)\\ \ddot{\zeta} &= G(\dot{\xi},\dot{\zeta},\zeta,\xi)\end{aligned}\right\} \qquad A.4$$

From the Kutta-Simpson one-third rule, Equations A. 4 can be expressed as a generalized set of simultaneous differential equations

$$\left.\begin{aligned}\frac{dP}{dt} &= f(P, \bar{P}, x, y)\\ \frac{d\bar{P}}{dt} &= g(P, \bar{P}, x, y)\end{aligned}\right\} \quad \text{where } P = \frac{dx}{dt},\ \bar{P} = \frac{dy}{dt}$$

or

$$\left.\begin{aligned}\frac{dP}{dt} &= F(P, \bar{P}, \xi, \zeta)\\ \frac{d\bar{P}}{dt} &= G(P, \bar{P}, \xi, \zeta)\end{aligned}\right\} \quad \text{where } P = \frac{d\xi}{dt},\ \bar{P} = \frac{d\zeta}{dt}$$

Using the generalized Runge-Kutta method (15)

$$\Delta P = \frac{1}{6}(\Delta' P + 2\Delta'' P + 2\Delta''' P + \Delta'^{v} P)$$
$$\Delta \bar{P} = \frac{1}{6}(\Delta' \bar{P} + 2\Delta'' \bar{P} + 2\Delta''' \bar{P} + \Delta'^{v} \bar{P})$$
$$\Delta x = \frac{1}{6}(\Delta' x + 2\Delta'' x + 2\Delta''' x + \Delta'^{v} x)$$
$$\Delta y = \frac{1}{6}(\Delta' y + 2\Delta'' y + 2\Delta''' y + \Delta'^{v} y)$$
$$\Delta' P = f(P_0, \bar{P}_0, x_0, y_0)$$
$$\Delta'' P = f(x_0 + \tfrac{1}{2}\Delta' P h,\ \bar{P}_0 + \tfrac{1}{2}\Delta' \bar{P}_0,\ P_0 + \tfrac{1}{2}\Delta' P_0,\ y_0 + \tfrac{1}{2}\Delta' \bar{P}_0 h)\, h$$
$$\Delta''' P = f(x_0 + \tfrac{1}{2}\Delta'' P h,\ \bar{P}_0 + \tfrac{1}{2}\Delta'' \bar{P}_0,\ P_0 + \tfrac{1}{2}\Delta'' P_0,\ y_0 + \tfrac{1}{2}\Delta'' \bar{P}_0 h)\, h$$
$$\Delta'^{v} P = f(x_0 + \tfrac{1}{2}\Delta''' P h,\ \bar{P}_0 + \tfrac{1}{2}\Delta''' \bar{P}_0,\ P_0 + \tfrac{1}{2}\Delta''' P_0,\ y_0 + \tfrac{1}{2}\Delta''' \bar{P}_0 h)\, h$$

$\Delta'\bar{P}$---$\Delta^{IV}\bar{P}$, $\Delta'x$---$\Delta^{IV}x$ and $\Delta'y$---$\Delta^{IV}y$ are found similarly to the $\Delta'P$---$\Delta^{IV}P$.

All the Δ'S must be found first, then all the Δ'' and so on.

Therefore, at t = h + o

$$P = P_o + \Delta P \qquad \text{and} \qquad x = x_o + \Delta x$$
$$\bar{P} = \bar{P}_o + \Delta\bar{P} \qquad\qquad y = y_o + \Delta y$$

This has been programmed for solution on an I.B.M. 7074 computer as described in Appendix II.

Calculation of the radius of the flame

The notations used here are defined as follows:

C	specific heat at constant pressure	$Btu/lb_m\,°F$
M	initial gas mass (air-acetylene)	lb_m
m_b	burned gas mass	lb_m
n	fraction of burned gas = $\frac{m_b}{M}$. $o \le n \le 1$	———
R	radius of the chamber	in.
T	temperature °R	———
V	volume of the chamber	$in.^3$
Y_b	radius of the flame	in.
V_b	volume of burned gas	$in.^3$
α	C_u/C_b	———

(subscripts u and b are unburned and burned gas respectively)

When the process can be assumed to be an isotropic process, as in our case, Campell (9) derived

$$n = \frac{\alpha - \left(\frac{P}{P_i}\right) + (1-\alpha)\left(\frac{P}{P_i}\right)^{\sigma_u}}{\alpha - \left(\frac{P_e}{P_i}\right) + (1-\alpha)\left(\frac{P_e}{P_i}\right)^{\sigma_u}} \qquad A.5$$

$$\sigma_u = \frac{\gamma_u - 1}{\gamma_u}$$

$$\gamma_u = \frac{C_{bu}}{C_{vu}}$$

$$\alpha = \frac{C_u}{C_b}$$

When this equation is not sensitive to the value of α which is true in our case, the simple equation $n = \frac{P - P_i}{P_e - P_i}$ is correct to within 3% for practical purposes.

The initial mass is given by

$$M = \frac{P_o V}{R T_o} \qquad R : \text{Gas constant} \qquad A.6$$

and the volume of the burned gas is given by

$$V_b = V - M(1-n)\frac{R T_u}{P} \qquad A.7$$

Substituting Equation A. 6 into Equation A. 7 we have

$$V_b = V\left[1 - \frac{T_u}{T_o}\frac{P_o}{P}\frac{P_e - P}{P_e - P_o}\right] \qquad A.8$$

then

$$\frac{V_b}{V} = \frac{r_b^2}{R^2} = \left[1 - \frac{T_u}{T_o}\left(\frac{P_o}{P}\right)\frac{P_e - P}{P_e - P_o}\right] \qquad A.9$$

Now in an isentropic process we can write

$$T_u = T_0 \left(\frac{P}{P_0} \right)^{\sigma_u}$$

Therefore

$$\frac{T_u}{T_0} = \left(\frac{P}{P_0} \right)^{\sigma_u} \qquad \text{A.10}$$

Substituting Equation A. 10 into Equation A. 9, we have for the radius of the flame as a function of chamber pressure and time

$$r_b = R_c \left[1 - \left(\frac{P_0}{P} \right)^{\frac{1}{\Gamma_u}} (1-n) \right]^{\frac{1}{2}} \qquad \text{A.11}$$

This is Equation 2. 11 in Chapter II which was used to determine the radius of the flame for use in the flame trajectory equations. Equations 2. 9, 2. 10, and 2. 16.

APPENDIX II

COMPUTER PROGRAM FOR EVALUATING THE NUMERICAL SOLUTION

Since a hand solution of the Equations 2.9 and 2.10 in Chapter II would have been too laborious, it was decided to use the University's computer, an I.B.M. 7074.

The program for the solution of the equation by the generalized Runge-Kutta method was written in Fortran language. This enabled the program to be written in essentially the same way as the algebraic solution, if the letters were written in stepwise fashion.

Nomenclature for I.B.M. 7074 Fortran Program

X = X
Y = Y — for fixed and rotational coordinates

XDOT = V_x
YDOT = V_y — velocity component on the X and Y axes for fixed and rotational coordinates

E = $\rho a D / \mu$

R: radius of the flame

ABSV = $\sqrt{\dot{x}^2 + \dot{y}^2}$ or $\sqrt{\dot{\xi}^2 + \dot{\zeta}^2}$

ABSR = $\sqrt{X^2 + Y^2}$ or $\sqrt{\xi^2 + \zeta^2}$

The remaining symbols are self-evident from the program logic.

FORTRAN PROGRAM

```
                    Compile Run Fortran
                    Dimension R(250), E(250)
C                   Flame Trajectory Version 1
                    Call Copy B (2)
      1             Print 501
    501             Format (1H 76H Trajectory of Flame and Its
                    Experimental Determination in Vortex Combustion)
      2             Read 552, N, OMEG, DT, TMAX, MMAX
    552             Format (110, 3F10.0, 110)
                    If(OMEG) 20, 20, 22
     22             Print 502, N
    502             Format (1HO, 4HN=, 14)
                    Read 551, (R(M), M=1, MMAX)
                    Read 551, (E(M), M=1, MMAX)
    551             Format (8F10.0)
      3             Print 503
    503             Format (1HO, 3X, 1HT, 12X, 4HXDOT, 13X, 4HYDOT,
                    15X, 16X, 1HY, 14X, 4HABS1V, 13X, 4HABSR, 14X
                    3HY/X)
      4             I=0
      5             T=0.0
                    X=0.625
                    Y=0.0
                    VX=0.0
                    VY=0.625*OMEG
```

FORTRAN PROGRAM, Continued

```
 6      T=FLOATF(1)*DT
        PT=1000.0*T
        ABSV=SQRTF(VX**2+VY**2)
        ABSR=SQRTF (X**2+Y**2)
        TANG=Y/X
 7      Print 505, PT, VX, VY, X, Y, ABSV, ABSR, TANG
505     Format (1HO, LX, F4. 2, 3X, 7E17. 8)
 8      J=1
 9      SDVX=0.0
        SDVY=0.0
        SDX=0.0
        SDY=0.0
        B=1.0
        C=0.0
10      TT=T+C*DT
        VJC+VX+C*DVJX
        VJY+VY+C*DVJY
        XJX=X+C*DXJX
        XJY=Y+C*DXJY
21      M-TT
        FM=FLOATF(M)
        M1=M+1
        M2=M+2
        RIJ=R(M1)+((R(M2)-R(M1))*(TT=FM))*1000.0
        EIJ=E(M1)+((E(M2)-E(M1))*TT-FM))*1000.0
```

FORTRAN PROGRAM, Continued

```
      RE=EIJ*SQRTF((VJX+XJY*OMEG)**2+(VJY-XJX*
      OMEG)**2)
200   IF(RE-0.1)100,101,201
201   IF(RE-1.0)101,102,202
202   IF(RE-10.0)102,103,203
203   IF(RE-1000.0)103,104,204
204   IF(RE-200000.0)104,105,205
206   IF(RE-1000000.0)106,107,107
100   DC=100.0
      Go to 11
101   CD-10.0*RE**(-0.782)
      Go to 11
102   CD=10.0*RE**(-0.552)
      Go to 11
103   CD=0.557*RE**(0.239)
      Go to 11
104   CD=RE**0.0634/0.647
      Go to 11
105   CD=25.4*RE**(-0.238)
      Go to 11
106   CD=0.02*RE**0.212
      Go to 11
107   CD=0.0
 11   DVJX=(-3.0*CD/(3.14159*RIJ)*SQRTF((VJX+
      XJY*OMEG)**2+(VJY-XJX*OMEG)**2)*(VJX+
      XJY*OMEG**2)*DT
```

FORTRAN PROGRAM, Continued

```
      DVJY=(-3.0*CD/(3.14159*RIJ)*SQRTF((VJX+
     XJY*OMEG)**2+(VJY-XJX*OMEG)**2)*(VJX-
     XJX*OMEG)-3.0*XJY*OMEG**2)*DT

      DXJX=VJX*DT+0.5*DVJX*DT**2

      DXJY=VJY*DT+0.5*DVJY*DT**2

12    SDVX=SDVX+B*DVJX

      SDVY=SDVY+B*DVJY

      SDX=SDX+B*DXJX

      SDY=SDY+B*DXJY

13    Go to (14, 16, 15, 17), J

14    B=2.0

      C=0.5

      Go To 16

15    B=1.0

      C=1.0

16    J=J+1

      Go To 10

17    VX=VX+0.16666667*SDVX

      VY=VY+0.16666667*SDVY

      X=X+0.16666667*SDX

18    TEST=TT+DT-TMAX

      IF(TEST)19, 2, 2

19    I=I+1

      Go to 6

20    Call Copy E

      Stop
      End
```

The basic program given here was used for the solution of Equations 2.9, 2.10 and 2.16 for the flame trajectories recorded in Fig. 4.16, 4.17, 5.4. The only change necessary in the program was in statement 11, which required a change in mathematical operations depending upon which equation was being solved.

Following is a tabulation of the constants used on the 10 data cards required in the previous Fortran Program. These data cards were the same for each of the three equations solved.

```
                 90094. 20000000. 000100000. 02200000        23

                 0. 000000000. 300000000. 440000000. 530000000
                 . 6000000000. 655000000. 7080000000. 76000000

R                0. 808000000. 852000000. 894000000. 930000000
                 . 970000001. 000000001. 034000001. 06000000

                 1. 090000001. 120000001. 150000001. 17600000
                 1. 200000001. 220000001. 24000000

                 0. 0000000027. 500000037. 000000044. 5000000
                 50. 500000056. 00000061. 00000066. 0000000

                 70. 500000074. 500000077. 600000080. 8000000
                 83. 000000085. 000000086. 500000086. 5000000
E
                 87. 500000086. 000000083. 500000079. 0000000
                 83. 000000054. 000000038. 500000

                 1800188. 4000000. 0001000000. 00600000      7

R                0. 000000000. 40000000. 70000000. 94000000
                 1. 060000001. 140000001. 20000000

E                0. 0000000034. 500000067. 500000083. 7000000
                 101. 40000097. 500000054. 0000000
```